

# Dipolar redistribution of summertime tropical cyclone genesis between the Philippine Sea and the northern South China Sea and its possible mechanisms

Joo-Hong Kim,<sup>1</sup> Chang-Hoi Ho,<sup>2</sup> and Pao-Shin Chu<sup>3</sup>

Received 7 April 2009; revised 4 November 2009; accepted 10 November 2009; published 20 March 2010.

[1] Recent observational records show that the dipole oscillation between the Philippine Sea (PS) and the northern South China Sea (nSCS) is a leading empirical orthogonal function (EOF) of summertime tropical cyclone (TC) genesis in the western North Pacific (WNP). This PS-nSCS oscillation is characterized by a distinguished decadal variability in addition to an interannual variability. Meanwhile, the typical El Niño–Southern Oscillation (ENSO)-related mode is found in the second EOF mode, which is predominantly interannual. With regard to the PS-nSCS oscillation, its interannual component appears to be linked with the previous wintertime ENSO event, but the linkage is not so robust in the sense that about half of its significant events are classified as the ENSO-related case, whereas its decadal component is coupled to a sea surface temperature anomaly (SSTA) in the central Pacific with its equatorial core near the Niño-4 region, which is flanked by an opposite SSTA on both sides along the latitudinal belt. Interestingly, this SSTA pattern resembles that related to the ENSO Modoki, and equivalently, the transitional phase of ENSO. The ENSO Modoki is regionally manifested by the anomalous zonal SST gradient between the equatorial western and central Pacific; thus the decadal modulation of this anomalous zonal SST gradient can be regarded as an actual forcing that forms and modulates the decadal PS-nSCS oscillation. In addition, the decadal PS-nSCS oscillation is compared with the decadal basin-wide TC genesis variation in terms of the Pacific SSTA pattern and the associated anomalous large-scale environments.

**Citation:** Kim, J.-H., C.-H. Ho, and P.-S. Chu (2010), Dipolar redistribution of summertime tropical cyclone genesis between the Philippine Sea and the northern South China Sea and its possible mechanisms, *J. Geophys. Res.*, 115, D06104, doi:10.1029/2009JD012196.

## 1. Introduction

[2] El Niño–Southern Oscillation (ENSO) has been receiving increased attention since the mid-1980s, because it is the most outstanding phenomenon that influences, in a very robust way, the year-to-year variability of seasonal tropical cyclone (TC) activity in the western North Pacific (WNP) (see *Chu* [2004] for a review). During the warm phase of ENSO, the WNP monsoon trough expands eastward as a low-level cyclonic Rossby wave response to the anomalous active convection near the date line; this response is associated with the positive sea surface temperature anomaly (SSTA) in the equatorial central/eastern Pacific (CP/EP). Accordingly, the preferred region of TC genesis also shifts to the southeast, adjacent to the date line. As a

result, those TCs can persist for longer periods in the WNP warm-pool region, receiving more thermal energy from the ocean surface and thereby possessing a longer lifespan and an increased intensity [*Wang and Chan*, 2002; *Camargo and Sobel*, 2005]. This situation is reversed during the cold phase of ENSO. Note that with regard to seasonal TC genesis, the apparent variability related to ENSO is the displacement of the preferred genesis region. However, the seasonal frequency of WNP TC genesis has a weak relationship with ENSO [*Lander*, 1994].

[3] In addition to the interannual variability, it has been found from long-term data records that WNP TC activity also varies on a decadal [*Yumoto and Matsuura*, 2001; *Matsuura et al.*, 2003] to an interdecadal time scale [*Chan and Liu*, 2004; *Ho et al.*, 2004; *Wu et al.*, 2005; *Chan*, 2006; *Liu and Chan*, 2008; *Chan*, 2008]. With respect to TC genesis, a main challenge has been to understand the underlying mechanism that modulates the frequency of seasonal genesis on the decadal time scale. The mechanism proposed by *Matsuura et al.* [2003] is the decadal ENSO-like coupled ocean-atmosphere feedback over the tropical Pacific. In this mechanism, the SSTA persistent throughout the decade over the tropical central North Pacific has a positive effect

<sup>1</sup>Met Office Hadley Centre, Exeter, UK.

<sup>2</sup>School of Earth and Environmental Sciences, College of Natural Sciences, Seoul National University, Seoul, South Korea.

<sup>3</sup>Department of Meteorology, School of Ocean and Earth Science and Technology, University of Hawai'i at Manoa, Honolulu, Hawaii, USA.

## 1st (Contour) and 2nd (Shading) EOF modes of TC genesis (1970–2007)

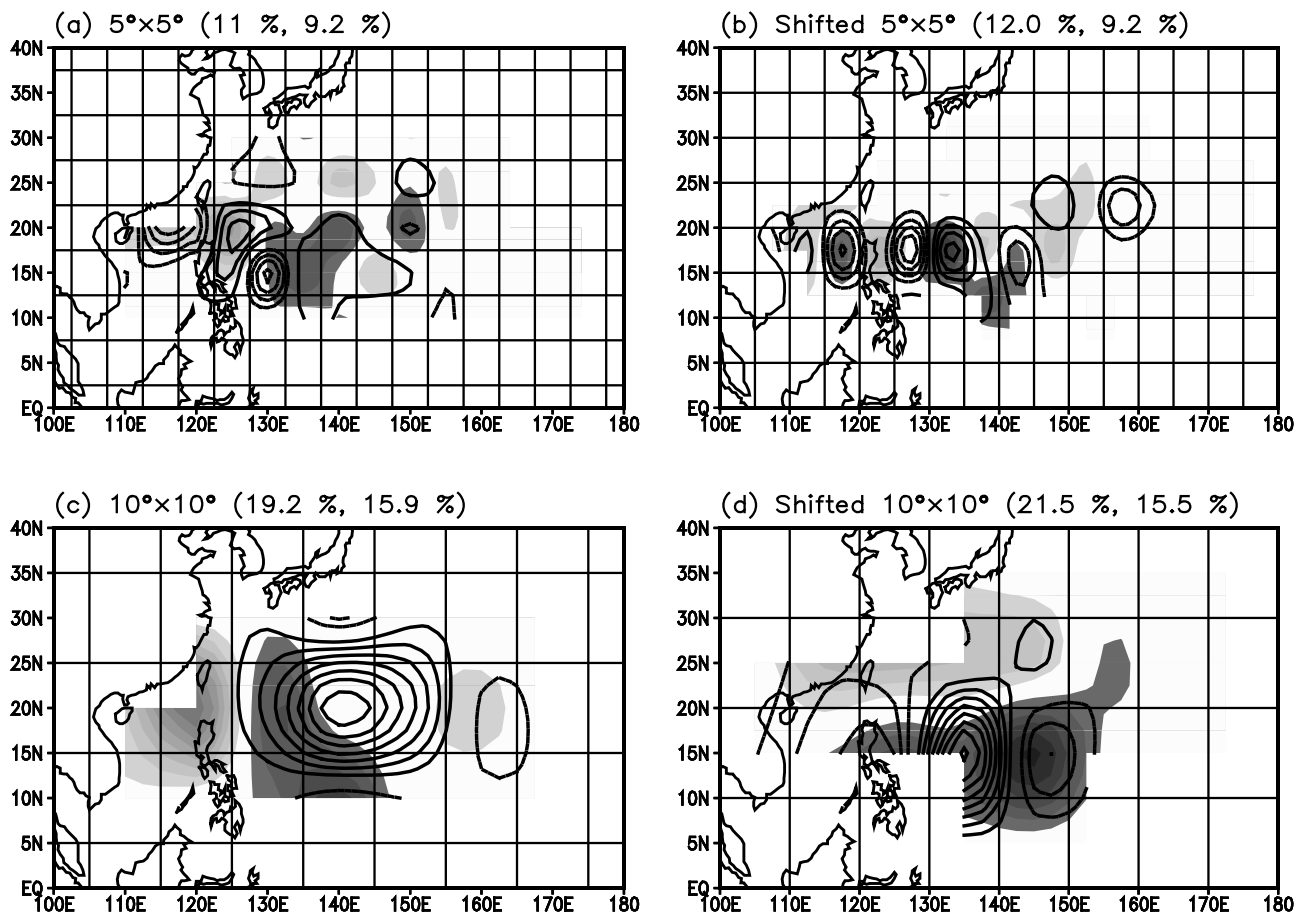


**Figure 1.** The first (contour) and second (shading) EOF modes of summertime TC genesis for the period from 1970 through 2007, discretely gridded with (a)  $5^\circ \times 5^\circ$  box, (b)  $5^\circ \times 5^\circ$  box shifted by  $2.5^\circ$  in latitude and longitude, (c)  $10^\circ \times 10^\circ$  box, and (d)  $10^\circ \times 10^\circ$  box shifted by  $5^\circ$  in latitude and longitude. Zero contours are omitted. The horizontal and vertical lines delineate grid boxes.

on the anomalous westerlies over the tropical WNP; subsequently, a low-level cyclonic vorticity prevails over the main development region of TCs, resulting in more TCs throughout the decade. This mechanism indicates that, similar to the interannual modulation of the preferred location of genesis, the decadal frequency modulation of WNP TC genesis is also affected by remote SST forcing.

[4] Even though the proposed mechanisms are similar to each other, there is a difference in their aspects of variability in TC genesis. With respect to the interannual time scale, both the seasonal basin-wide frequency and the sub-basin-scale redistribution have been explored in relation to ENSO. With respect to the decadal time scale, however, only the seasonal basin-wide frequency, not the sub-basin-scale redistribution, has been reported in the literature. Naturally, this leads to several questions as follows:

[5] 1. Is there variability that is representative of a sub-basin-scale decadal redistribution of WNP TC genesis?

[6] 2. If such variability exists, is it merely a regional manifestation of the decadal variability in basin-wide TC genesis that has been reported so far?

[7] 3. If the decadal redistribution is distinctive from the decadal variability in basin-wide TC genesis, what is its structural difference, and what physical mechanisms does it owe to its existence?

[8] To provide relevant answers to the above questions, the authors address this issue by applying conventional empirical orthogonal function (EOF) analysis to the gridded summertime (July, August, and September) TC genesis. The EOF analysis reveals two characteristic leading modes of spatiotemporal variability: one is a newly found dipole oscillation, having a clear decadal fluctuation as well as an interannual one, between the Philippine Sea (PS) and the northern South China Sea (nSCS); the other is a well-known ENSO-related oscillation between the northern PS and the southeastern WNP adjacent to the date line. Indeed, the PS-nSCS-oriented dipole mode, compared to ENSO-related mode, has a distinctive property related to ENSO. In this study, we discuss the physical background of this dipole mode and its relationship with the known decadal variability in basin-wide seasonal TC genesis.

[9] The remainder of this paper is organized as follows: Section 2 describes the data used and discusses the gridding

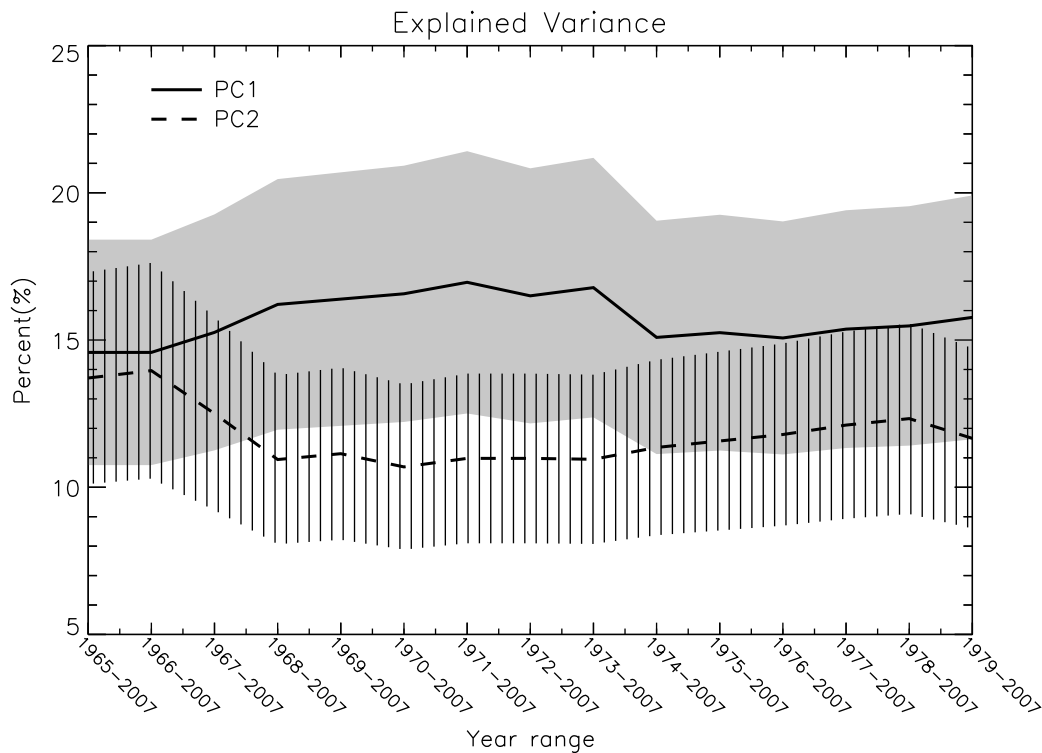


**Figure 2.** The series of the explained variance (%) with their confidence limits for first mode (solid line with gray shading) and second mode (dashed line with vertical hatches). The starting year has been chosen from the period 1965 through 1979 with 1 year increments.

method of TC genesis. Section 3 presents the two leading EOFs for WNP TC genesis. Section 4 addresses the large-scale environments corresponding to the two EOFs and also to the basin-wide TC genesis, with the discussions being focused on the interannual and decadal time scales separately. Finally, section 5 presents summary and concluding remarks.

## 2. Data and Gridding Technique

### 2.1. Data

[10] The information regarding WNP TC genesis was obtained from the Regional Specialized Meteorological Centers–Tokyo Typhoon Center. The data cover the period from 1951 through 2007. The location where an individual TC first attains tropical storm intensity (i.e.,  $v_{\max} \geq 17 \text{ m s}^{-1}$ ) is set as the genesis point, so that the TCs include both tropical storms and typhoons. It is possible that TC genesis points near the CP would not have been detected in the presatellite era (before the mid-1960s). To avoid this problem, only the TC information in the weather satellite era (1965–2007) was used in this study [Wang and Chan, 2002]. In addition, we included only the data for the summer months of July, August, and September in our analysis, a period during which more than 60% of TCs develop. We concentrated on the summer season mainly to isolate the influence of seasonal changes on the location of TC genesis in the EOF analysis.

[11] We also used the extended reconstructed SST data from the National Oceanic and Atmospheric Administration (NOAA) [Smith and Reynolds, 2004], outgoing longwave

radiation (OLR) data [Liebmann and Smith, 1996], and data for horizontal winds at 850 and 200 hPa from the National Centers for Environmental Prediction/National Center for Atmospheric Research (NCEP/NCAR) [Kalnay *et al.*, 1996]. While using the same period for the SST and horizontal winds that was used for the TC data, the availability of the continuous OLR data set confines the common period from 1979 to the present.

[12] The Pacific Decadal Oscillation (PDO) [Mantua *et al.*, 1997] index was provided by the Joint Institute for the Study of the Atmosphere and Ocean in the University of Washington. The PDO index is defined as the leading principal component (PC) time series of monthly SSTA in the North Pacific Ocean poleward of  $20^{\circ}\text{N}$ .

### 2.2. Data Gridding Technique

[13] Our study used EOF analysis, which requires the data to be gridded before they can be processed further. So far, TC data gridding has usually been performed by binning the latitude and longitude positions into a grid box of a discrete size (e.g.,  $5^{\circ} \times 5^{\circ}$ ) [cf. Kim *et al.*, 2005; Liu and Chan, 2008]; this method has been generally applied to the binning of track information. However, if TC genesis points in each season were binned directly, their numbers are much fewer than track frequency, leaving many grids with zeroes even with such a large grid size. When we perform the EOF analysis with this data, even the leading modes are turned out to be spatially noisy and physically meaningless patterns in terms of climate time scales (Figure 1a). To make matters worse, the EOF modes come out quite differently with the gridded data whose grid centers are artificially shifted

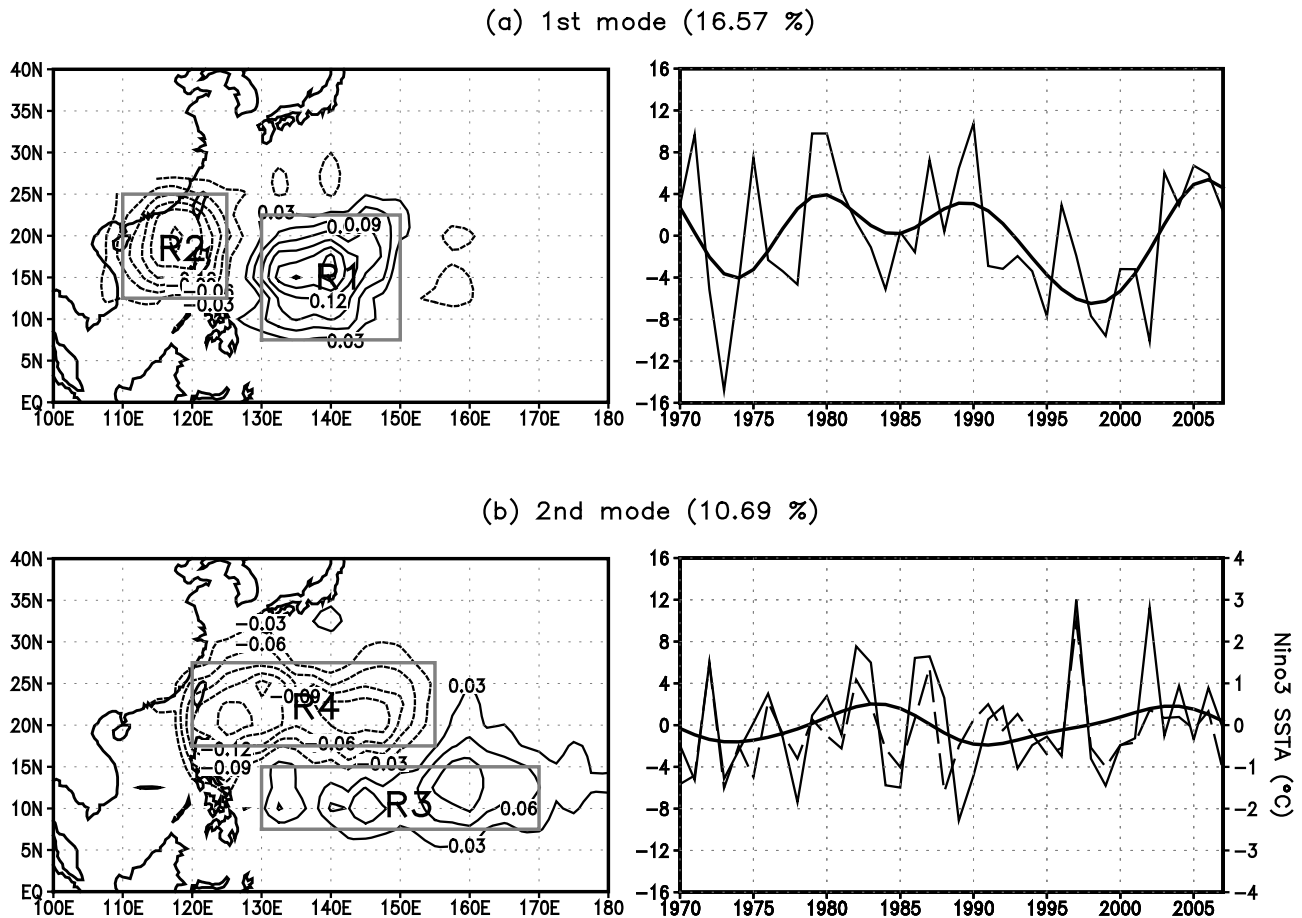


**Figure 3.** The (a) first and (b) second EOFs and the associated PC time series of summertime TC genesis obtained from data for the period from 1970 through 2007. Low-pass-filtered (period > 10 year) values of the PC time series are demonstrated as thick solid lines. The rectangular boxes in the EOF plot indicate the defined regions of interest. The dashed line shown with the second PC time series indicates the Niño-3 index. The unit of EOF is arbitrary and that of PC time series is number.

(Figure 1b). One way to filter out the noise may be to enlarge the size of a grid box, thus we show the results with  $10^\circ \times 10^\circ$  gridded data in Figures 1c and 1d. As a matter of course, the spatial pattern becomes quite simpler. One unambiguous improvement, compared to Figures 1a and 1b, is that the first mode in Figure 1c and the second mode in Figure 1d are physically interpretable as an ENSO-related spatial variation in that their PC time series are well correlated with Niño indices (figure not shown). However, the change in spatial patterns by shifting the grid center is still a big problem. In fact, this effect can be diminished only by lessening the grid size. Here a problem arises that two issues (i.e., spatial noise versus shift in the grid center) are incompatible with each other.

[14] It is inevitable to make a finer resolution with applying the spatial smoothing to overcome this numerical problem. Thus, we binned all the genesis points for each summer into a  $10^\circ \times 10^\circ$  latitude-longitude grid window (kernel); to bin the genesis points within the window, we successively shifted this window at  $2.5^\circ$  intervals in latitude and longitude. Using the raw latitude-longitude genesis points result in gridded genesis data having a  $2.5^\circ \times 2.5^\circ$  horizontal resolution. By filling up the grids around the genesis points with nonzero

smoothed values, this so-called “overlap-gridding” technique smoothes the sporadic TC genesis points in a domain. This method is believed to settle the problem arising from the discrete gridding technique. To verify this, we decide to check whether the EOF modes resulting from the overlap-gridding method demonstrated any artificiality caused by the spatial smoothing. To this end, we examined the actual TC genesis time series in and around the cores of variability revealed by the EOF analysis. When the actual time series accurately represents the variability extracted by the analysis, this confirms that a physical mode is operating.

### 3. Two Leading EOFs for WNP TC Genesis

[15] To extract the leading eigenmodes that are representative of spatiotemporal variability in summertime WNP TC genesis, we applied the conventional EOF analysis technique to the gridded seasonal TC genesis fields. In order to test whether the leading EOF patterns are robust, regardless of the length of the period of interest, we performed EOF analyses repeatedly, using data starting from different years within the weather satellite era to the present. The starting years were chosen successively from 1965 through 1979. The

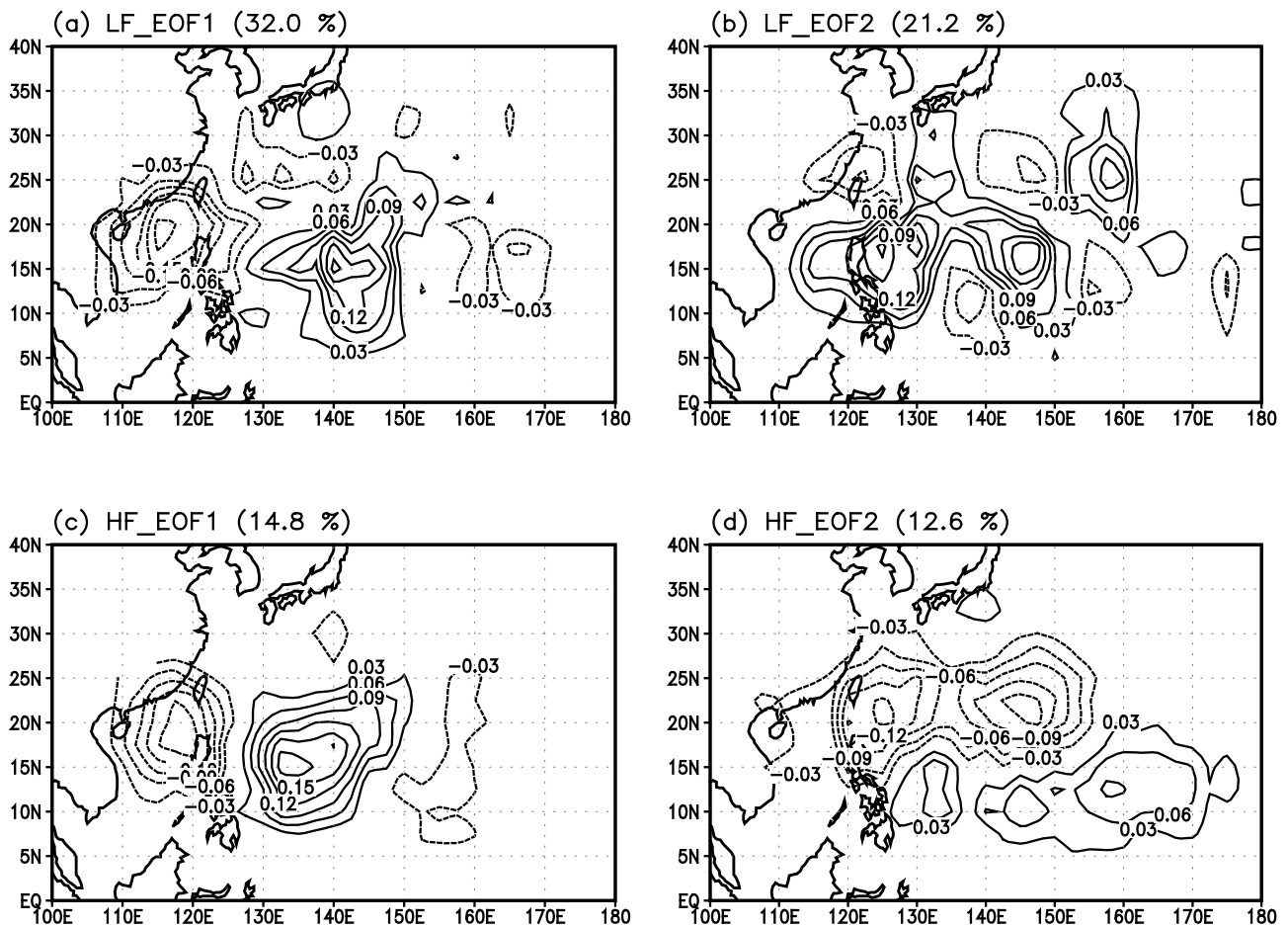


**Figure 4.** The (left) first and (right) second EOF modes of summertime TC genesis for the period from 1970 through 2007, calculated with (a, b) low-pass-filtered data and (c, d) high-pass-filtered data (period < 10 year).

results show a robust dipole oscillation pattern between the PS and the nSCS as a first EOF mode with varying explained variances (figure not shown). The explained variances of the first mode are largest when the EOF analysis is performed with starting years of around 1970 (Figure 2). During this period, the first modes are relatively well separated from the second mode, even though all of them fail to attain a complete separation beyond a 95% confidence error limit of the rule of thumb [North *et al.*, 1982]. The fact that two modes are not statistically separable based on the rule of thumb does not mean that they are (sentences the results to be) completely unphysical, but rather means a possible distortion of the real pattern. Unfortunately, it is not possible to clear this doubt by increasing the sample size due to the limited reliable data. Instead, we insist the physical existence of this mode a posteriori because it is always found as a leading mode in all the EOF analyses with any time period and any time length, as well as it clearly appears in the real TC data (e.g., Figures 5a, 10, and 16). Because there is a negligible difference in the subsequent analyses no matter which period we choose, we address the data period from 1970 through 2007 in the remainder of this discussion.

[16] Figure 3a shows the first EOF pattern and its PC time series for the data period from 1970 through 2007. This PC time series exhibits large variability on the decadal time

scale as well as the interannual one. We believe that this PS-nSCS dipole oscillatory mode in WNP TC genesis has not been documented in the previous literature. On the other hand, the second EOF seems to exhibit the typical ENSO-related spatial redistribution in WNP TC genesis (Figure 3b), not only in that the location of the two poles of variability resembling the TC shifts during warm and cold ENSO events but also in that the significant linear correlation ( $r = 0.74$ ) of its PC time series with the summertime Niño-3 index.

[17] To further confirm the two leading modes, the EOF analysis is separately applied to the interannual (high-pass-filtered, period < 10 year) and decadal (low-pass-filtered, period > 10 year) TC genesis data (Figure 4). The PS-nSCS dipole oscillatory mode is revealed as a first mode on both interannual and decadal time scales. The PS-nSCS mode is more pronounced against the second mode on the decadal time scale, whereas it has a comparable explained variance to the second mode that can be regarded as the ENSO-related mode. If the two EOF modes have a comparable explained variance, they can represent one physical mode in different phase [Zhang and Hendon, 1997]. Actually, it will be shown in section 4 that the first EOF on the interannual time scale is also related to the phase change of ENSO.

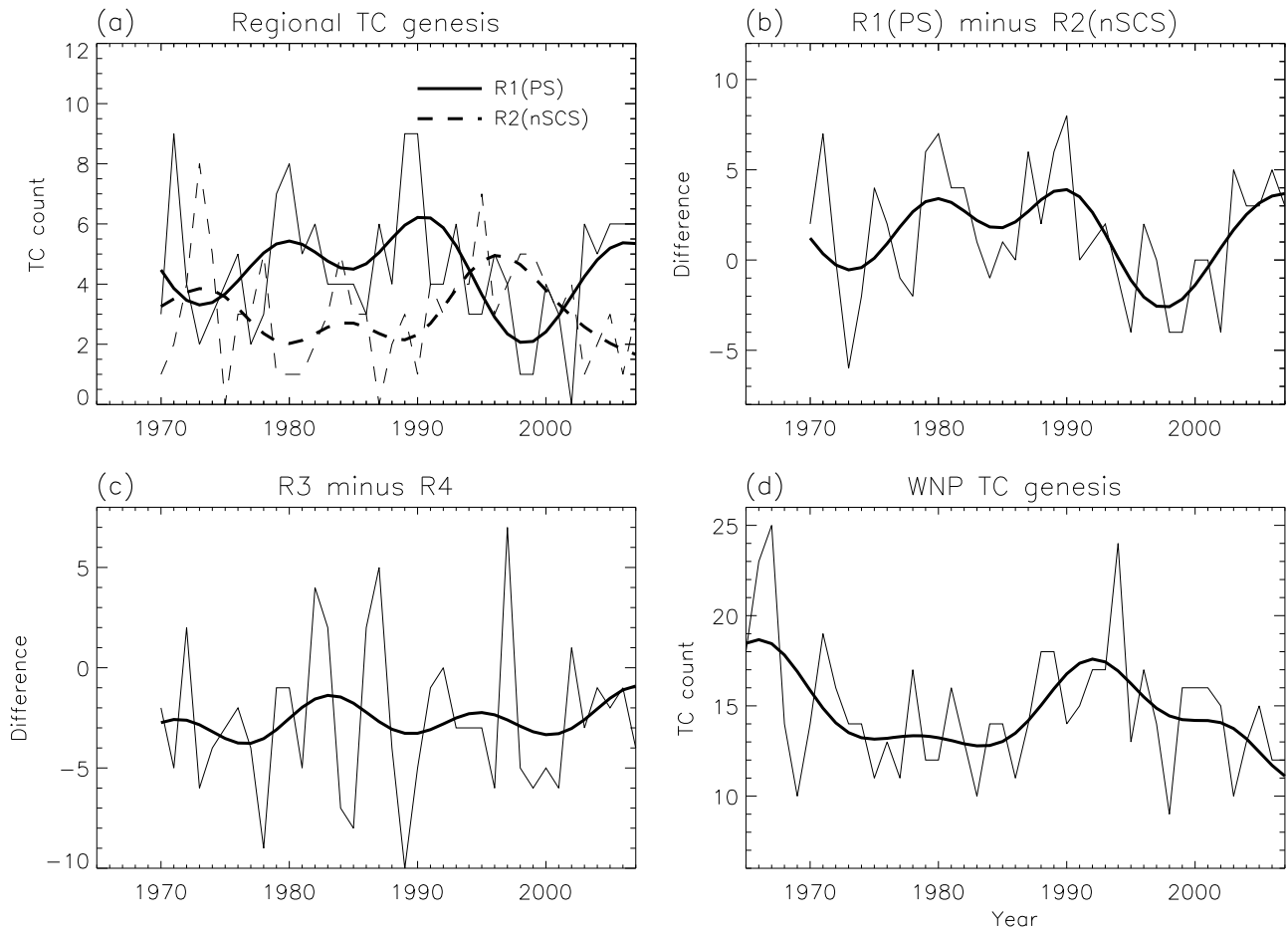


**Figure 5.** The unfiltered (thin line) and the low-pass-filtered (thick line) time series of summertime TC genesis for the period from 1970 through 2007: (a) summed over the region R1 (PS; solid line) and R2 (nSCS; dashed line); (b) difference between R1 and R2 (the PS-nSCS oscillation); (c) difference between R3 and R4 (the typical ENSO-related oscillation); and (d) basin-wide summertime WNP TC genesis for the period from 1965 through 2007.

[18] Two core regions are defined to confirm how robustly the redistribution of summertime TC genesis between the PS and the nSCS is observed in the raw data set: the rectangular region 1 (R1,  $130^{\circ}$ – $150^{\circ}$ E,  $7.5^{\circ}$ – $22.5^{\circ}$ N) encloses one pole over the PS, while the region 2 (R2,  $110^{\circ}$ – $125^{\circ}$ E,  $12.5^{\circ}$ – $25^{\circ}$ N) encloses the other over the nSCS (Figure 3a). In addition, we chose region 3 (R3,  $130^{\circ}$ – $170^{\circ}$ E,  $7.5^{\circ}$ – $15^{\circ}$ N) and region 4 (R4,  $120^{\circ}$ – $155^{\circ}$ E,  $17.5^{\circ}$ – $27.5^{\circ}$ N) in terms of the ENSO-related variability for comparison with the PS-nSCS dipole mode (Figure 3b). Figure 5a depicts a time series of summertime TC genesis in two domains, R1 and R2, during the period from 1970 through 2007. As expected, the two time series show an approximately inverse relationship with a linear correlation of  $-0.57$ . On a decadal time scale, this inverse relationship is even more evident. When a Lanczos filter is used, the correlation coefficient between two low-pass-filtered time series is  $-0.78$  [Duchon, 1979]. There is indeed a strong redistribution of WNP TC genesis between the PS and the nSCS. Figure 5b shows the difference of two regions (i.e., R1 minus R2), which can be used as a reference time series to extract the large-scale environments connected to the PS-nSCS dipole oscillation. The percentage of variance explained by decadal

fluctuation ( $\sigma_{\text{decadal}}^2/\sigma^2$ ) is about 31% in this time series. For comparison, to represent the spatial variation associated with ENSO, we also constructed a time series of the difference between R3 and R4 (Figure 5c). This time series will be referred to as the typical ENSO-related oscillation hereafter. Compared to the PS-nSCS oscillation, this time series has more interannual variability with a relatively weaker decadal fluctuation ( $\sigma_{\text{Decadal}}^2/\sigma^2 \sim 6.5\%$ ); its correlation coefficient with the summertime Niño-3 index is 0.77, which is as large as that obtained from the PC time series. Also shown is the time series of summertime TC genesis frequency in the WNP with low-pass-filtered values (Figure 5d). We used the low-pass-filtered one as a reference time series to extract the regressed large-scale environments afterward.

[19] The PS-nSCS dipole oscillation was clearly seen in the raw independent time series over R1 and R2 (Figure 5a). However, it is still questionable as to whether only the dipole oscillation is clearly distinguishable in relation to the first EOF mode or the other oscillatory patterns are mixed with it. To help answer this question, we show the independent correlation maps of basin-wide TC genesis with the time series of TC genesis over R1 and R2, respectively (Figure 6). The large negative correlation coefficients are

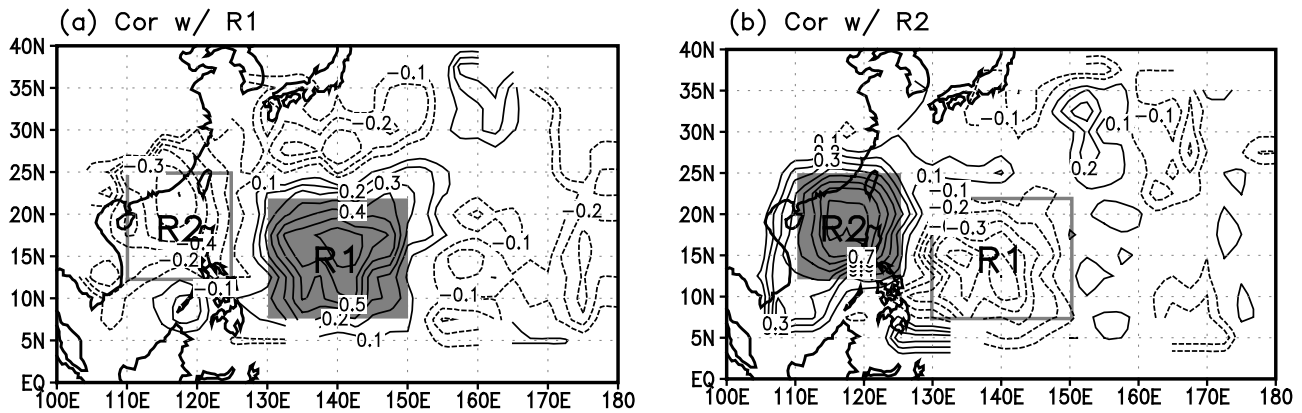


**Figure 6.** Correlations of basin-wide summertime TC genesis for the period from 1970 through 2007 with respect to the time series of TC genesis over (a) R1 and (b) R2.

only found in R2 when the basin-wide TC genesis is correlated with the R1 time series, and vice versa, indicating that the PS-nSCS dipole is not mixed with other possible oscillations during the periods when it dominates the summertime WNP TC genesis.

#### 4. Large-Scale Patterns Corresponding to the Two EOF Modes

[20] Because the Indo-Pacific SST variability is one of the main factors affecting climate variability over the WNP, it is beneficial to examine the SST variations in order to understand how the leading EOF modes of WNP TC genesis are linked to large-scale environments. The interannual SST variability in the Indo-Pacific is manifested by the ENSO phenomenon, whereas the decadal SST variability, whose patterns and origins are complex and in debate, is manifested either by the PDO [Mantua *et al.*, 1997], by the tropical Pacific ENSO-like decadal variability [Lohmann and Latif, 2005], by the North Pacific mode [Nakamura *et al.*, 1997; Barlow *et al.*, 2001], or by the North Pacific Gyre Oscillation [Di Lorenzo *et al.*, 2008]. This led us to examine the two time scales separately to analyze of the large-scale fields with respect to the high-pass-filtered (the solid line in Figure 8) and the low-pass-filtered (the thick line in Figure 5b) reference time series of the PS-nSCS oscillation, respectively. However, we did not apply the time filter to the reference time series of the typical ENSO-related oscillation (Figure 5c) because it is predominantly interannual.

##### 4.1. Interannual Variability

[21] Figure 7 presents the lead and lag regression of seasonal mean SSTs upon the high-pass-filtered reference time series of the PS-nSCS oscillation (the thin line minus the thick line in Figure 5b, i.e., the solid line in Figure 8), as well as the reference time series of the typical ENSO-related oscillation (the dashed line in Figure 8) for the period from 1970 through 2007. From the seasonal evolution in Figure 7a, the decaying years of El Niño or La Niña seem to be related to the year-to-year variability of the PS-nSCS oscillation; that is., the frequency of TC genesis tends to increase in the PS (nSCS) when the previous wintertime La Niña (El Niño) decays in the following spring and summer. This was our expectation that we presumed in the EOFs using the high-

pass-filtered TC genesis data (Figure 4c). It is interesting to note that the high-frequency variability of the PS-nSCS oscillation is associated with ENSO, especially with its decaying phase. However, we admit this relation may be less robust than that with the developing phase of ENSO because of the following two reasons: first, the overall statistical significance in the tropical SST evolution from the previous fall through the summer is less than 99% confidence level using student's *t* test, and second, there is no significant contemporaneous relationship with the Indian Ocean SST variability in summer. As is well known, the tropical Indian Ocean experiences a basin-wide warming after an El Niño episode [Klein *et al.*, 1999; Xie *et al.*, 2009]. Thus, if the low phase of the PS-nSCS oscillation were tightly associated with the El Niño decaying summer, a trace of an organized SSTA must be detected in the Indian Ocean. On the other hand, there is a distinct developing basin-wide SST variability both in the Indian Ocean and the Pacific when the seasonal SSTs are regressed upon the typical ENSO-related oscillation (Figure 7b).

[22] How many years are explained in association with the decaying phase of ENSO among the total high or low years of the interannual PS-nSCS oscillation? To answer this question, Figure 8 presents the standardized interannual PS-nSCS oscillation (the solid line) as well as the typical ENSO-related oscillation (the dashed line) together. The El Niño (“E”) and La Niña (“L”) years are marked based on the wintertime SSTA from the Climate Prediction Center/NOAA (available on the Web via [http://www.cpc.noaa.gov/products/analysis\\_monitoring/ensostuff/ensoyears.shtml/](http://www.cpc.noaa.gov/products/analysis_monitoring/ensostuff/ensoyears.shtml/)). There are a total of 10 high ( $\geq 0.5\sigma$ , i.e., 1971, 1975, 1979, 1980, 1987, 1989, 1990, 1996, 1997, and 2003) and 13 low ( $\leq -0.5\sigma$ , i.e., 1973, 1974, 1977, 1978, 1984, 1986, 1988, 1991, 1992, 1995, 1998, 1999, and 2002) events of the interannual PS-nSCS oscillation with seven of high events (i.e., 1971, 1975, 1980, 1987, 1990, 1996, and 2003) being higher than  $1\sigma$  and seven of low events (i.e., 1973, 1977, 1978, 1984, 1991, 1993, and 2002) being lower than  $-1\sigma$ . Among the 10 high events, four (marked with open and filled circles) are associated with the previous wintertime La Niña event (i.e., 4/10 for the total events), and as for the strong events ( $\geq 1\sigma$ ), three (marked with filled circles) among the 7 events are classified as the corresponding cases (i.e., 3/7 for the strong events). When it comes to the low

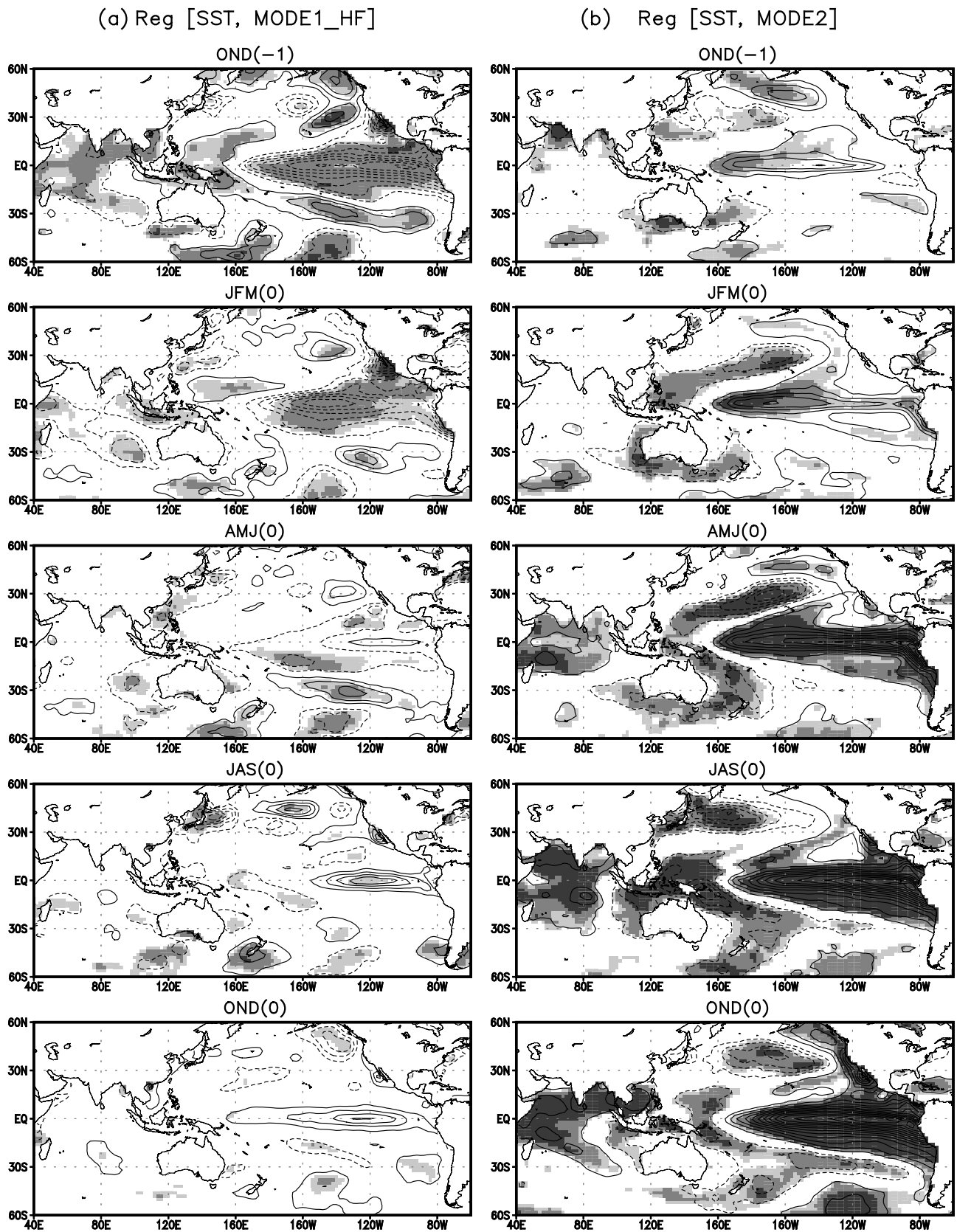


**Figure 7.** The lead and lag regressions of 3 month averaged SSTs upon (a) the high-pass-filtered PS-nSCS oscillation, as well as upon (b) the typical ENSO-related oscillation. The contour interval is  $0.02^{\circ}\text{C}$   $\text{Number}^{-1}$ . Zero contours are omitted. The light gray, gray, and dark gray shadings depict the significant regions at 90, 95 and 99% confidence levels, respectively.

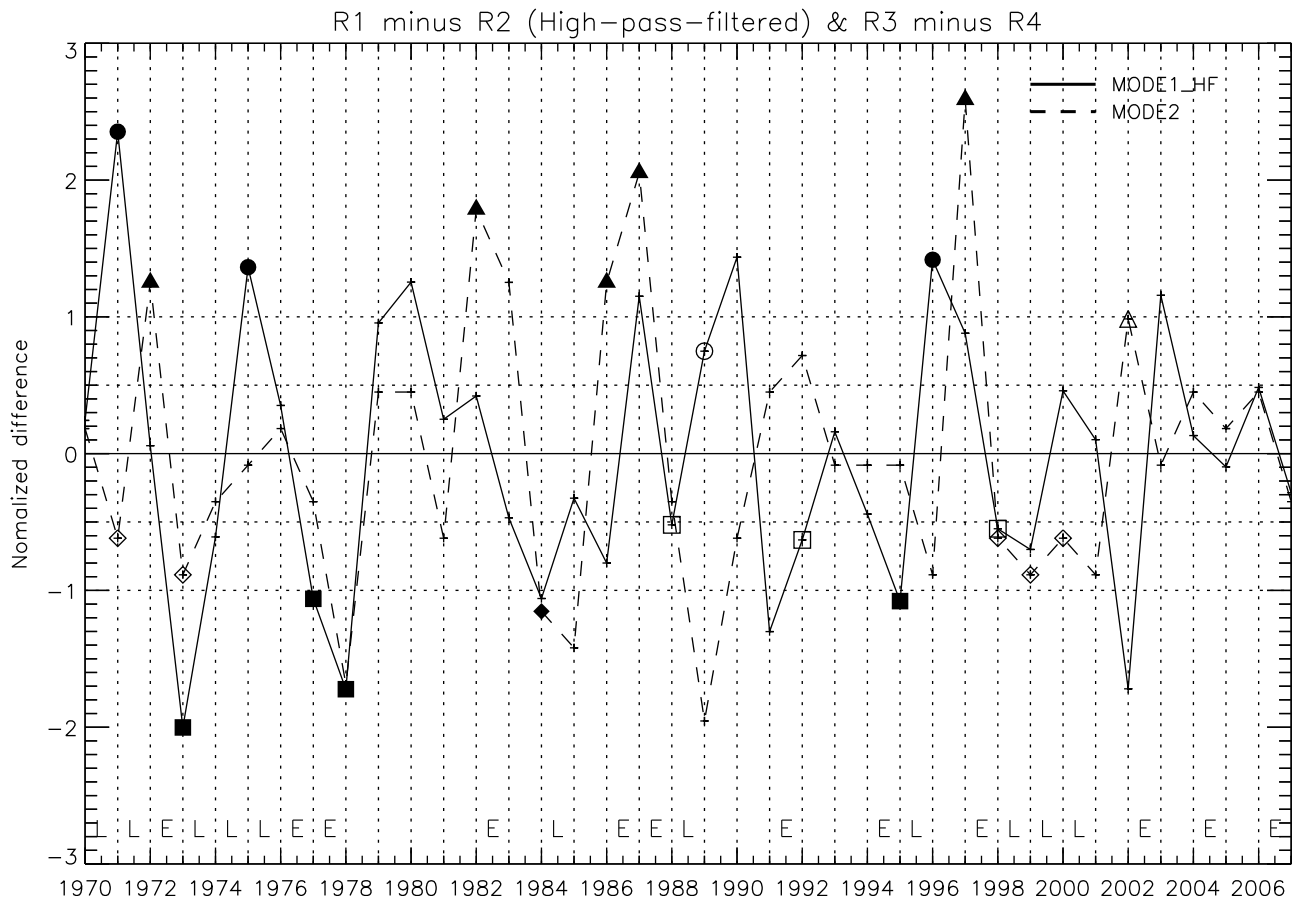


**Figure 8.** The high-pass-filtered PS-nSCS oscillation (solid line), and the typical ENSO-related oscillation (dashed line). The circle (square) marks are to indicate the years when the apparent PS-nSCS dipole signal (open symbol for  $1.0\sigma > \text{Normalized difference} \geq 0.5\sigma$ , filled symbol for  $\text{Normalized difference} \geq 1.0\sigma$ ) is found in relation to the previous wintertime La Niña, “L” (El Niño, “E”), whereas the triangle (diamond) marks are to indicate the years when the typical ENSO-related oscillation is found in relation to the following wintertime El Niño (La Niña). Horizontal dotted lines denote  $\pm 0.5\sigma$  and  $\pm 1.0\sigma$ .

events, seven (marked with open and filled squares) among the 13 low events (i.e., 7/13 for the total events) and four (marked with filled squares) among the 7 strong ( $\leq -1\sigma$ ) events (i.e., 4/7 for the strong events) are associated with the previous wintertime El Niño event, respectively. As a total, about half of the total (i.e.,  $(4 + 7)/(10 + 13)$ ) and strong events (i.e.,  $(3 + 4)/(7 + 7)$ ) are related to the previous wintertime ENSO event, indicating that the interannual PS-nSCS oscillation occurs either with or without the previous wintertime ENSO episode.

[23] For a comparison, we also count the number of high and low events associated with the typical ENSO-related oscillation (Figure 8). There are a total of 8 high and 13 low events; among them, six (i.e., 1972, 1982, 1983, 1986, 1987, and 1997) of high events are higher than  $1\sigma$  and only four (i.e., 1978, 1984, 1985, and 1989) of low events are lower than  $-1\sigma$ . Six events (marked with open and filled triangles) are identified in association with the El Niño developing phase (i.e., 6/8 for the total events) and five of them are the strong events (i.e., 5/6 for the strong events). When it comes to the La Niña developing phase, 6 events (marked with open and filled diamonds) among 13 low

events match the La Niña developing phase (i.e., 6/13 for the total events) and among the 6 La Niña-related events, only one is the strong event (marked with filled diamond) that happens associated with the La Niña development (i.e., 1/4 for the strong events). Different from the El Niño-related events, the La Niña-related events are much fewer in the number, indicating an asymmetry in the response of TC genesis to ENSO during its developing phase. As a total, slightly more than half of the total (i.e.,  $(6 + 6)/(8 + 13)$ ) and 60% of strong events (i.e.,  $(5 + 1)/(6 + 4)$ ) are related to the ENSO development. This is somewhat surprising because we expected much higher percentage explained by the ENSO episodes, compared to the interannual PS-nSCS oscillation.

[24] The relatively larger fraction of years corresponding to El Niño in the typical ENSO-related oscillation than that in the PS-nSCS oscillation is just what we have expected; however, the fraction corresponding to La Niña is similar to or less (for the strong events) than that in the PS-nSCS oscillation. Actually, the latter lessens the total linkage of the typical ENSO-related oscillation with ENSO events. This asymmetry between the El Niño and La Niña events results in the large discrepancy in the successive temporal

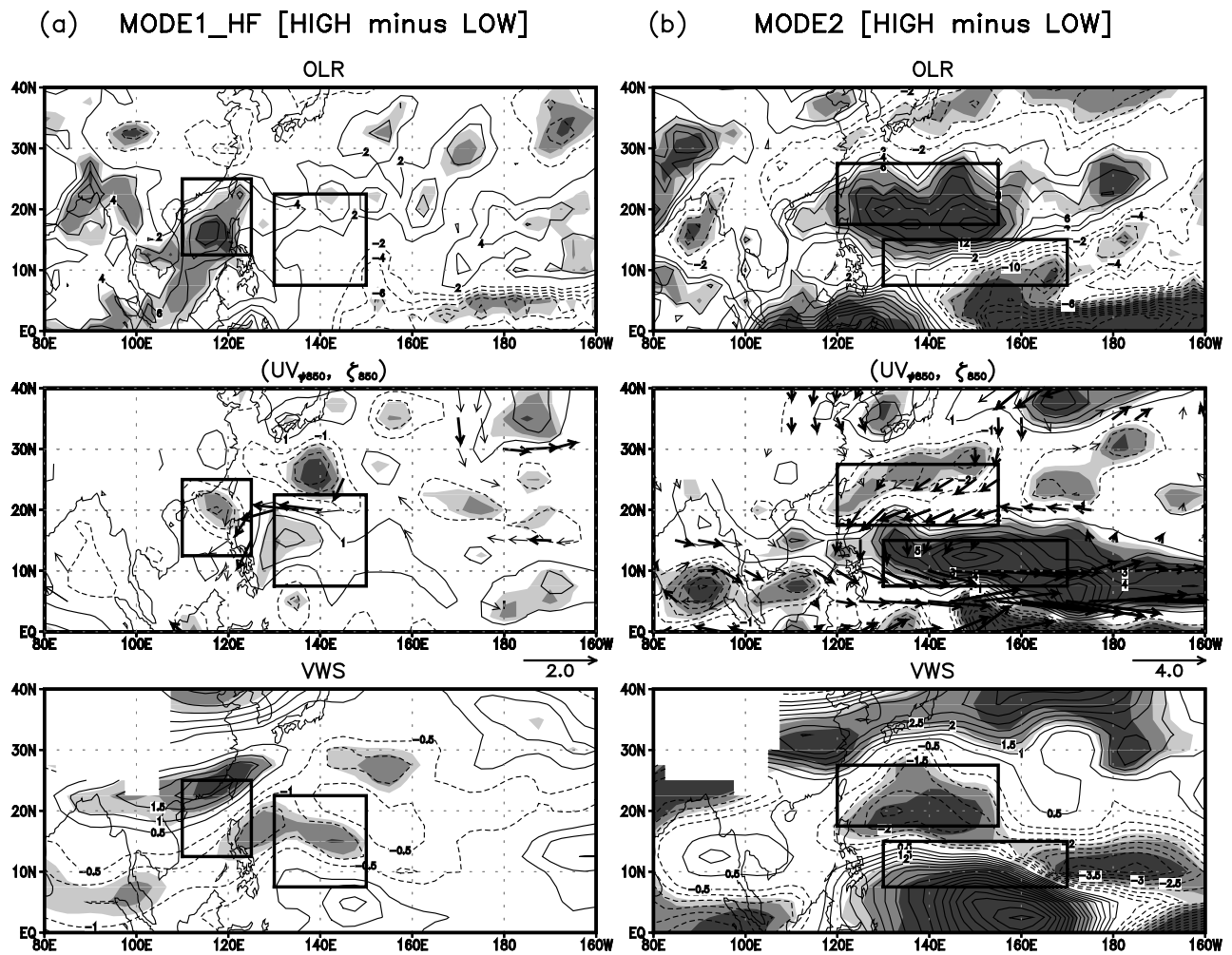


**Figure 9.** The composite difference maps of summertime averaged atmospheric variables ((top) OLR, (middle) 850 hPa rotational winds/relative vorticity, and (bottom) magnitude of vertical shear of horizontal winds) between the high ( $\geq 0.5\sigma$ ) and low ( $\leq -0.5\sigma$ ) years of (a) the high-pass-filtered PS-nSCS oscillation, as well as of (b) the typical ENSO-related oscillation. The period used is from 1970 through 2007 except for OLR from 1979 through 2007. The contour interval for the OLR is  $2 \text{ W m}^{-2}$ ; for the 850 hPa relative vorticity, it is  $10^{-6} \text{ s}^{-1}$ ; and for the magnitude of the vertical wind shear, it is  $0.5 \text{ m s}^{-1}$ . Zero contours are omitted. The light gray, gray, and dark gray shadings depict the significant regions at 90, 95, and 99% confidence levels, respectively. Only the significant wind vectors are plotted with thin (90%) and thick (95%) arrows. Four rectangular boxes are the same as those shown in Figure 3.

relationship between two time series. There is a nice coherency (i.e., the high phase of the typical ENSO-related oscillation in the previous year leads to the low phase of the PS-nSCS oscillation in the following year) before and after the four conventional El Niño events (i.e., 1972–1973, 1982–1983, 1987–1988, and 1997–1998). On the other hand, the successive years from the low phase of the typical ENSO-related oscillation to the high phase of the PS-nSCS oscillation (i.e., 1978–1979, 1989–1990, and 1996–1997) are just normal years. To synthesize all of these results lead us to the following conclusions. First, both the interannual PS-nSCS oscillation and the typical ENSO-related oscillation occur more tightly linked with the El Niño events rather than the La Niña events. Second, the interannual PS-nSCS oscillation is less robust in linkage with El Niño than the

typical ENSO-related oscillation, but its relation with La Niña remains much the same (or even stronger for the strong events) since the typical ENSO-related oscillation is also marginally related to La Niña.

[25] To extract the concomitant large-scale environments associated with their respective variability in the WNP TC genesis, the composite difference maps between the high ( $\geq 0.5\sigma$ ) and low ( $\leq -0.5\sigma$ ) years of the two reference time series (Figure 8) are shown in Figure 9 for the fields of summertime large-scale atmospheric environments: the OLR, the rotational winds and the relative vorticity at 850 hPa, and the magnitude of the vertical shear of horizontal winds (vertical wind shear). The vertical wind shear is defined as  $\sqrt{(u_{200} - u_{850})^2 + (v_{200} - v_{850})^2}$ , where  $u$  and  $v$

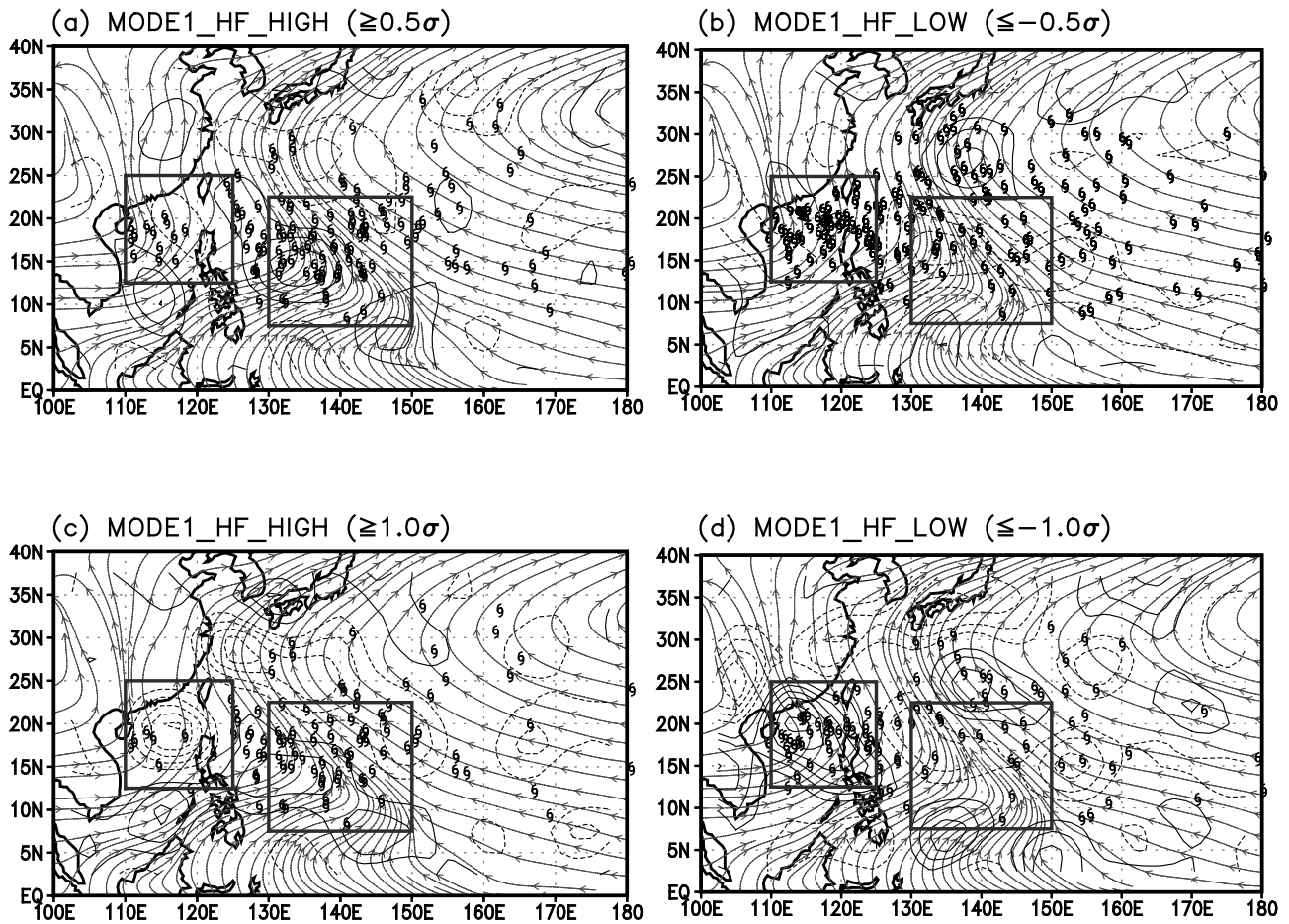


**Figure 10.** The composite maps of the 850 hPa horizontal winds (streamline) and the anomalous relative vorticity (contour, solid for positive values) for the years when the high-pass-filtered PS-nSCS oscillation is (a) higher than  $0.5\sigma$ , (b) lower than  $-0.5\sigma$ , (c) higher than  $1.0\sigma$ , and (d) lower than  $-1.0\sigma$ . Zero contours are omitted. The storm symbols are also plotted to locate TC genesis.

are zonal and meridional winds, respectively. Figure 9a presents the composite differences in terms of the interannual PS-nSCS oscillation. For the region of R1 (PS), the relative vorticity and vertical wind shear show significant anomalies consistent with the sign of anomalous TC genesis, but the OLR anomalies are not significant; that is, the favorable dynamic condition enhances (or reduces) TC genesis in the PS. Meanwhile, the significant anomalies in the OLR and relative vorticity are located within R2 (nSCS) and also the significant anomalies in the vertical wind shear overlaps in its northern part. All of these together explain the anomalous TC genesis in the nSCS. The dipolar pattern in the low-tropospheric relative vorticity corresponds nicely to the interannual PS-nSCS oscillation of TC genesis. The composite differences in terms of the typical ENSO-related oscillation show stronger and significant anomalies in the regions of interest (Figure 9b). While the anomalies in the relative vorticity exactly reside in R3, those in the OLR and vertical wind shear are found in R4. Note that the genesis variations in R3 are more attributed to the relative vorticity than the other two factors. *Wang and Chan [2002]* have also noticed that the increase of the low-level shear vorticity mainly attributes to

the enhanced TC genesis in the southeast quadrant of the WNP (i.e., R3).

[26] The vorticity dipole shown in Figure 9a suggests corresponding variations in the monsoon trough and subtropical high in the low troposphere. The composite maps of total fields of the low-tropospheric circulation are illustrated with the locations of TC genesis in Figure 10 to illustrate the roles of the monsoon trough and the subtropical high associated with the interannual PS-nSCS oscillation. During the high years (Figures 10a and 10c), the monsoon trough becomes more (less) cyclonic in the PS (nSCS) and the subtropical ridge along the  $30^{\circ}\text{N}$  becomes more anticyclonic. There is a pronounced redistribution of the number of TC genesis between two regions: 67 per 10 year (47 per 7 year) in the PS versus 16 per 10 year (8 per 7 year) in the nSCS for the thresholds of  $\pm 0.5\sigma$  ( $\pm 1.0\sigma$ ). The opposite is true during the low years (Figures 10b and 10d). However, the latter redistribution is a bit weaker due to less frequent genesis in the nSCS as well as more frequent genesis in the PS: 34 per 13 year (18 per 7 year) in the PS versus 59 per 13 year (36 per 7 year) in the nSCS with the thresholds of  $\pm 0.5\sigma$  ( $\pm 1.0\sigma$ ).

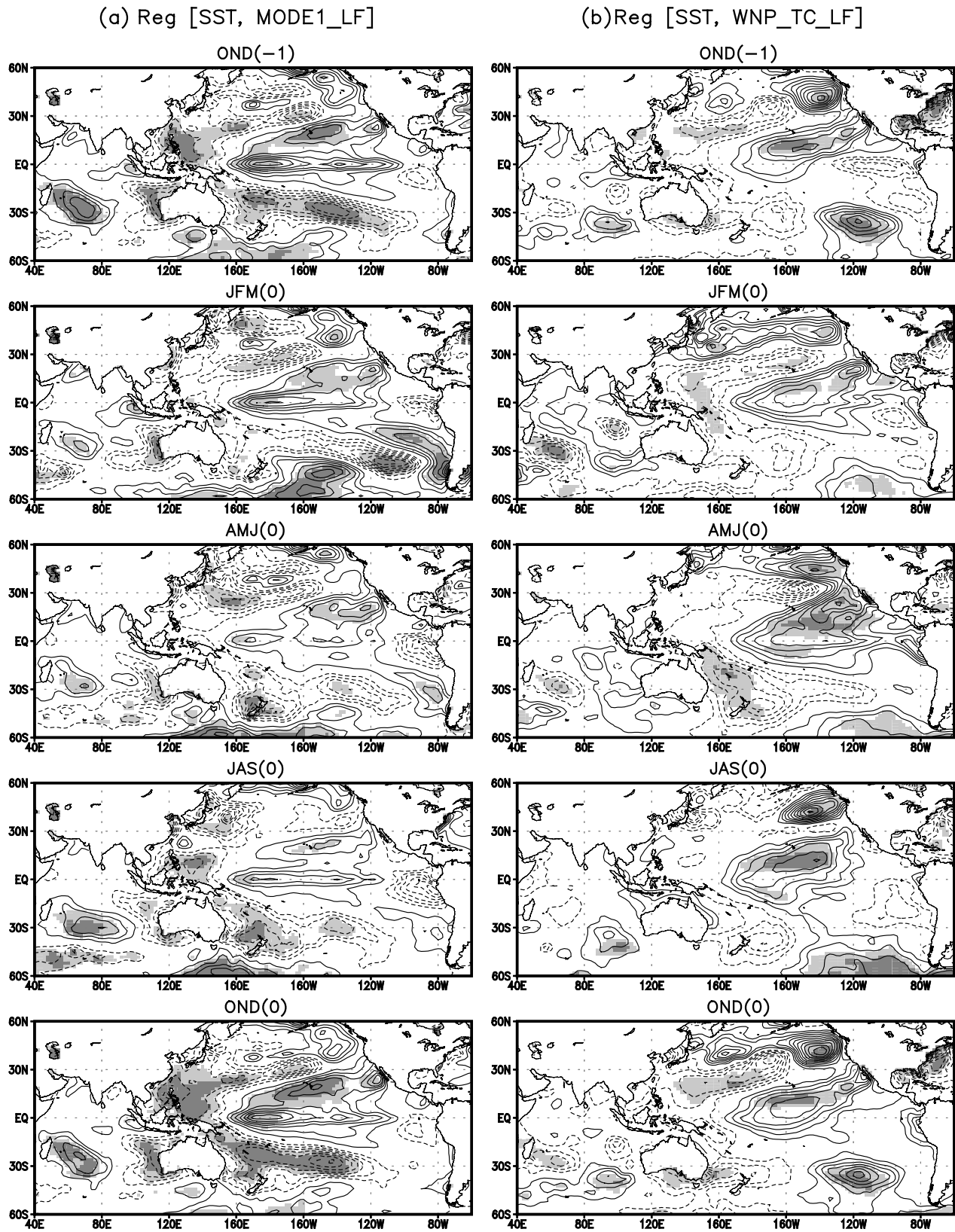


**Figure 11.** Same as Figure 7 except for the regressions upon (a) the low-pass-filtered PS-nSCS oscillation and (b) the low-pass-filtered time series of basin-wide summertime WNP TC genesis.

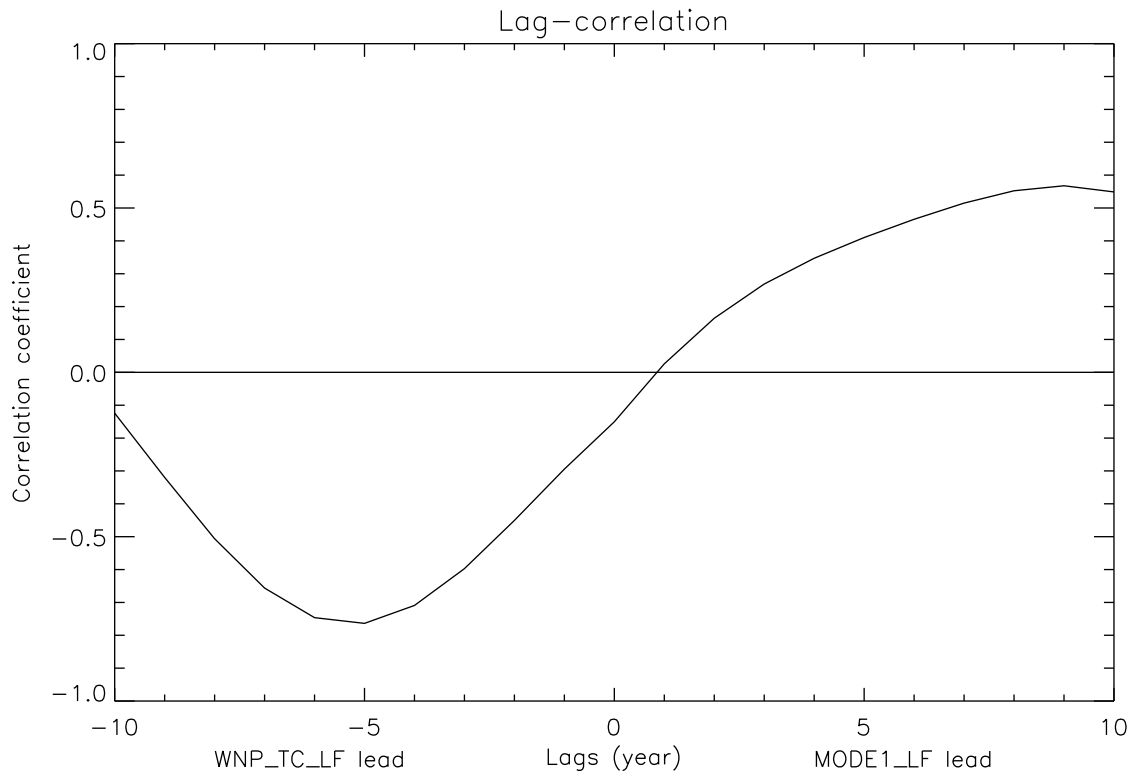


**Figure 12.** The lead and lag correlation coefficients of the low-pass-filtered PS-nSCS oscillation and the low-pass-filtered basin-wide summertime WNP TC genesis.

#### 4.2. Decadal Variability

[27] Figure 11 shows the lead and lag regressions of seasonal SSTs upon the low-pass-filtered time series of the PS-nSCS oscillation (the thick line in Figure 5b), as well as upon the low-pass-filtered time series of the basin-wide summertime TC genesis in the WNP (the thick line in Figure 5d). With respect to the decadal PS-nSCS oscillation, the homogeneous tropical SST pattern (warming (cooling) centered in the tropical CP with its equatorial core near the Niño-4 (160°E–150°W, 5°S–5°N) region, flanked by cooling (warming) on either side of the warming along the latitudinal belt) persists through the entire seasons (Figure 11a). On the other hand, all the regression patterns of seasonal SSTs upon the decadal variability of the basin-wide TC genesis are found to have spatially shifted anomalous center, which is located in slightly north of the equator extending northeastward toward the central American coast (Figure 11b). Based on the regressed SSTA pattern, it appears that two decadal modes of WNP TC genesis are shifted with respect to each other. To identify its possibility, we compute the lead and lag correlations of the two low-pass-filtered time series (Figure 12). The maximum negative correlation is found when the decadal variability of the basin-wide TC genesis leads that of the PS-nSCS oscillation by about 5 years. This suggests that the two representative decadal variations of WNP TC genesis may be connected with a different phase of the decadal variability in the Pacific SSTs. However, because it is not possible to substantiate this postulate without a longer-term model simulation, we should leave this subject for the future study.

[28] It is interesting to note that the decadal regression patterns upon the low-pass-filtered time series of the PS-nSCS oscillation (Figure 11a) are reminiscent of the ENSO Modoki (Pseudo-ENSO) phenomenon which has been discussed in the recent literature [Ashok *et al.*, 2007; Weng *et al.*, 2007; Chang *et al.*, 2008]. The ENSO Modoki index (EMI) is defined by subtracting half of the summed area-mean SSTA over the tropical western Pacific (WP; 125°–145°E, 10°S–20°N) and EP (110°–70°W, 15°S–5°N) from the area-mean SSTA in the tropical CP (165°E–140°W, 10°S–10°N) [Ashok *et al.*, 2007]. This index has a similar nature to the Trans-Niño index (TNI; the difference in normalized SSTA between the Niño-1 + 2 and the Niño-4 regions) [Trenberth and Stepaniak, 2001]. Because the TNI represents the zonal gradient in equatorial CP and EP SST, a gradient that characterizes the evolutionary (transitional) pattern of ENSO, so does the EMI. (The EMI has been newly termed because many of the recent CP warming events in the equatorial CP did not eventually develop into a canonical El Niño [see Ashok *et al.*, 2007].) This suggests that these indices are approximately orthogonal to the canonical ENSO indices which characterize the amplitude of ENSO (e.g., Niño-3.4 or Niño-3 index). That is, the high EMI (or negative TNI) period characterize the positive CP SSTA and also the negative WP and EP SSTA. The EMI exhibits a larger decadal spectral power than an interannual power [Weng *et al.*, 2007]. While in the tropical EP, the interannual variability is much larger than the decadal SST modulation, the decadal variability is particularly evident in the tropical WP and CP [Trenberth and

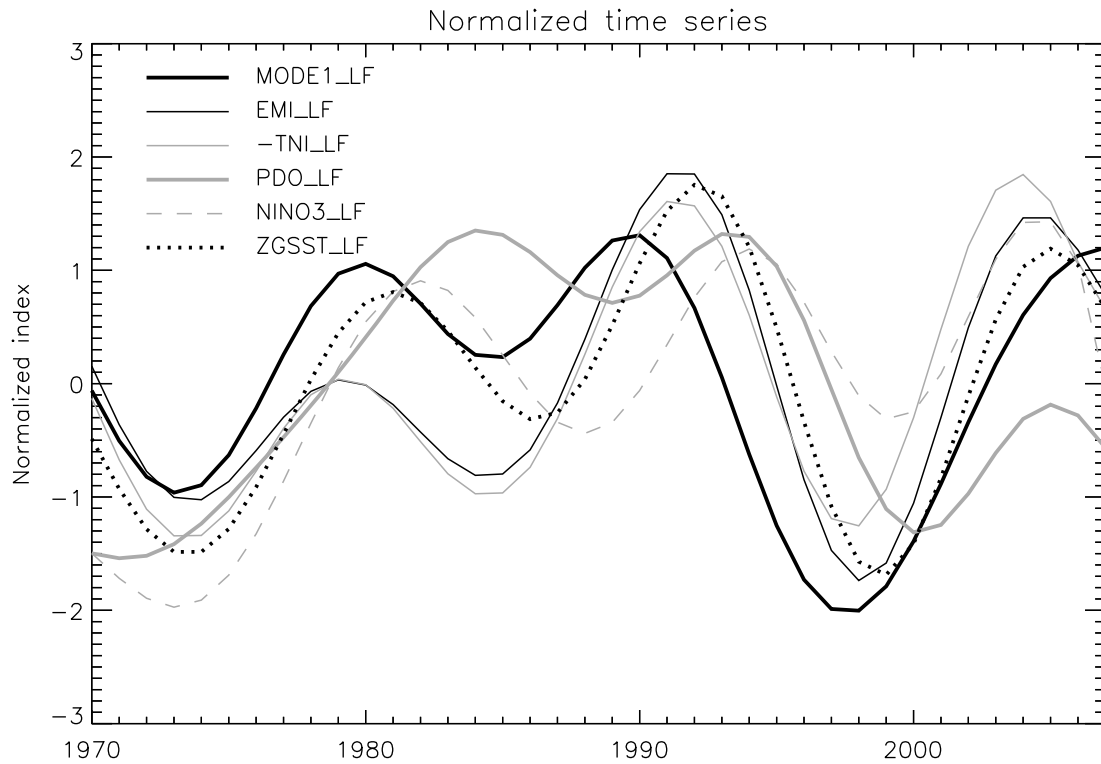


**Figure 13.** The normalized low-pass-filtered time series of the PS-nSCS oscillation (thick black solid line), EMI (thin black solid line), negative TNI (thin gray solid line), PDO index (thick gray solid line), Niño-3 index (thin gray dashed line), and ZGSST index (thick black dotted line) for the period from 1970 through 2007. Note that indices are plotted only with the values in summer.

Hurrell, 1994; Graham, 1994]. Thus, the WP and CP sub-components of the EMI are representative of its large decadal fluctuation. To characterize the tropical SST variability in the WP and CP, we define a new index based on Figure 11a, a normalized difference between the SST [160°E–120°W, 10°S–10°N] and SST [120°–145°E, 5°S–15°N], which expresses the zonal gradient of the SST (ZGSST) between the tropical WP and CP. In Figure 13, the low-pass-filtered time series of the PS-nSCS oscillation, EMI, negative TNI, ZGSST index, Niño-3 index and PDO index are plotted together for the period from 1970 through 2007. All indices refer to summertime only. The PDO index is added for a comparison with other indices of the tropical decadal oscillations. In addition, the cross  $r^2$  [ $n$ -lag] values in percent of these low-pass-filtered time series are listed in Table 1. As shown in Figure 13 and Table 1, the decadal PS-nSCS oscillation is a tolerably in-phase (though not perfectly in-phase) with the EMI ( $r^2$  [0] = 47%), negative TNI ( $r^2$  [0] = 31%) and ZGSST

index ( $r^2$  [0] = 52%), whereas the PDO index ( $r^2$  [0] = 19%,  $r^2$  [+3] = 51%) seem to lag behind the decadal PS-nSCS oscillation by a few years. The former is apparent because the decadal PS-nSCS oscillation has traces of the decadal variability of the ENSO transition. On the other hand, the latter implies that the annually persistent SSTA pattern in Figure 11a is followed by the PDO-type SSTA pattern [i.e., Mantua *et al.*, 1997, Figure 2a] during the analysis period. This phase lag is understandable in that the PDO is rather congruent with the decadal Niño-3 index ( $r^2$  [0] = 39%) representative of the ENSO amplitude, whereas the decadal PS-nSCS oscillation is more congruent with the indices representative of the ENSO transition. The ZGSST index is fairly well explained by the other indices (46%–76% within  $\pm 1$ -lag) with the largest  $r^2$  with the EMI and the negative TNI, indicating that it is more evident during the evolutionary phase of ENSO. Because this index was constructed within the WP and CP regions, it is more straightforward to

**Table 1.** The  $r^2$  Values of the Low-Pass-Filtered Time Series Pairs<sup>a</sup>

	MODE1_LF	EMI_LF	-TNI_LF	PDO_LF	Niño-3_LF	ZSSTG_LF
MODE1_LF		47%	31%	19%	7%	52%
EMI_LF	0-lag		89%	11%	22%	74%
-TNI_LF	0-lag	0-lag		5%	34%	61%
PDO_LF	51% at +3-lag	17% at +2-lag	10% at +2-lag		39%	46%
Niño-3_LF	10% at +1-lag	27% at +1-lag	42% at +1-lag	0-lag		54%
ZSSTG_LF	64% at +1-lag	76% at +1-lag	72% at +1-lag	52% at -1-lag	0-lag	

<sup>a</sup>The 0-lag  $r^2$  values are in the upper triangle, and the maximum  $r^2$  values with  $n$  year-lag ( $|n| \geq 1$ ) are in the lower triangle. The positive lag means the indices in the column lead those in the row.

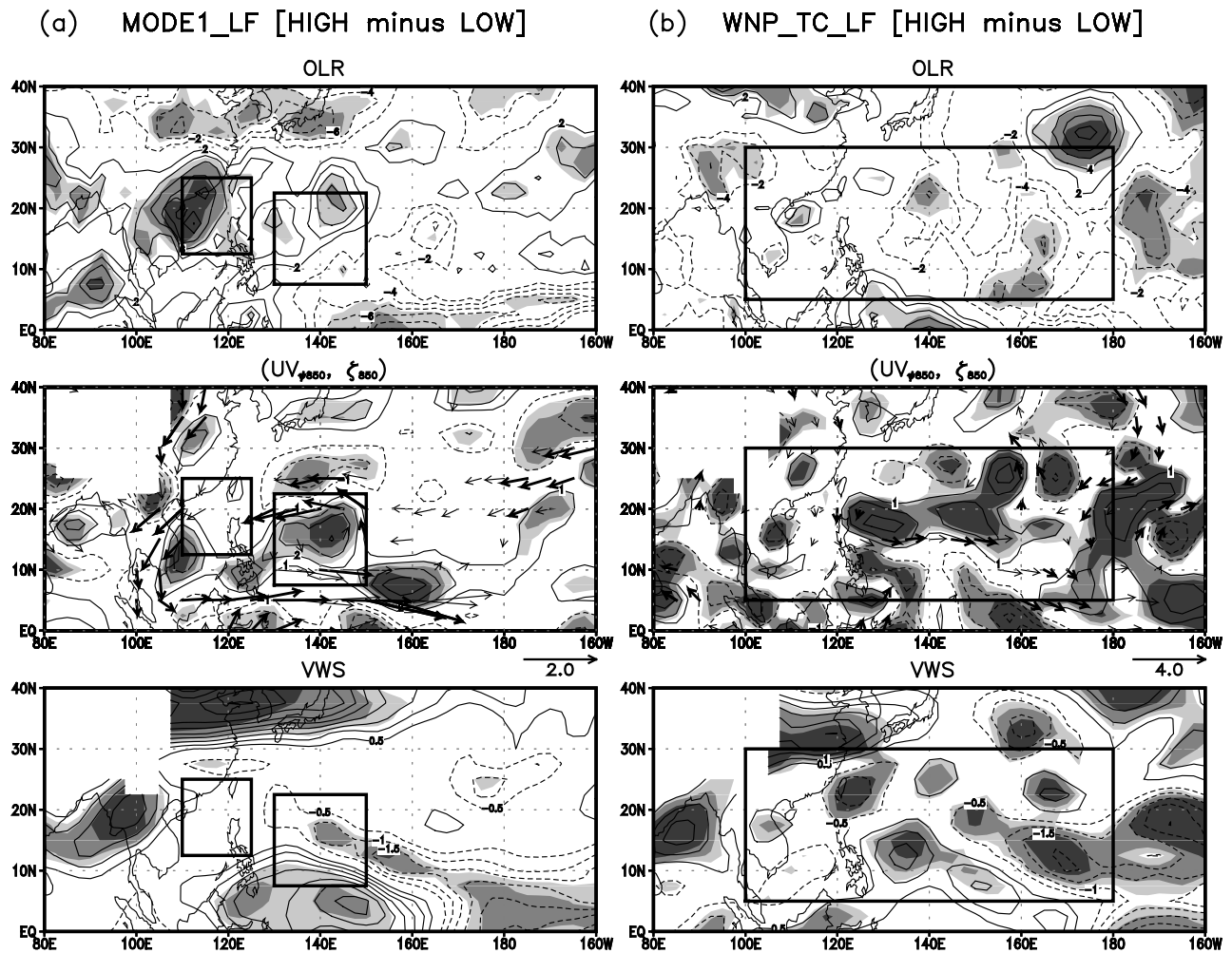


**Figure 14.** Same as Figure 9 except for (a) the low-pass-filtered PS-nSCS oscillation and (b) the low-pass-filtered basin-wide summertime WNP TC genesis. A box in Figure 14b represents main TC genesis region in the WNP.

explain the anomalous forcing driving the large-scale responses that render the decadal PS-nSCS oscillation. Taken together, these results suggest that the decadal PS-nSCS oscillation can be physically understood in line with the decadal variability of the tropical Pacific SST.

[29] The composite difference maps between the high ( $\geq 0.5\sigma$ ) and low ( $\leq -0.5\sigma$ ) years of the two reference time series are also shown for the decadal variability (Figure 14). Figure 14a presents the composite differences with respect to the decadal PS-nSCS oscillation (the thick line in Figure 5b). Similar to the interannual time scale, the OLR anomalies present a consistent signal with TC genesis only in the nSCS. On the other hand, the significant anomalies in the low-tropospheric relative vorticity and vertical wind shear are found only in the PS. That is, the dipolar signal can be expected only if the three variables were combined. We can speculate that the composites based on the low-pass-filtered time series are disturbed by the interannual variability, thus the dipolar structure of the large-scale variables may not be as apparent as in the decadal variability, or the primary mechanism that modulates TC genesis is different between the two

regions. It is interesting to note that the composite difference patterns are structurally similar to those associated with the typical ENSO-related oscillation (Figures 9b versus 14a), except for the zonal extent. In response to the weaker ZGSST in the tropical WP and CP regions, convective heating is enhanced in the equatorial WP as inferred from the negative OLR anomalies and the near equatorial anomalous westerlies are strengthened (Figure 14a, middle), forming the low-level anomalous cyclonic circulation in the PS. This is the qualitatively similar explanation as proposed by *Matsuura et al.* [2003] to explain the decadal modulation of the basin-wide TC genesis in the WNP. In this regard, it is necessary to compare the decadal PS-nSCS oscillation with the decadal variation in basin-wide TC genesis in order to reveal the differences in the large-scale environments between two distinctive variabilities.

[30] Figure 14b shows the composite differences with respect to the time series of the decadal basin-wide TC genesis (the thick line in Figure 5d). It is found that the OLR anomalies marginally support the corresponding variation in TC genesis. The other two dynamic variables also show

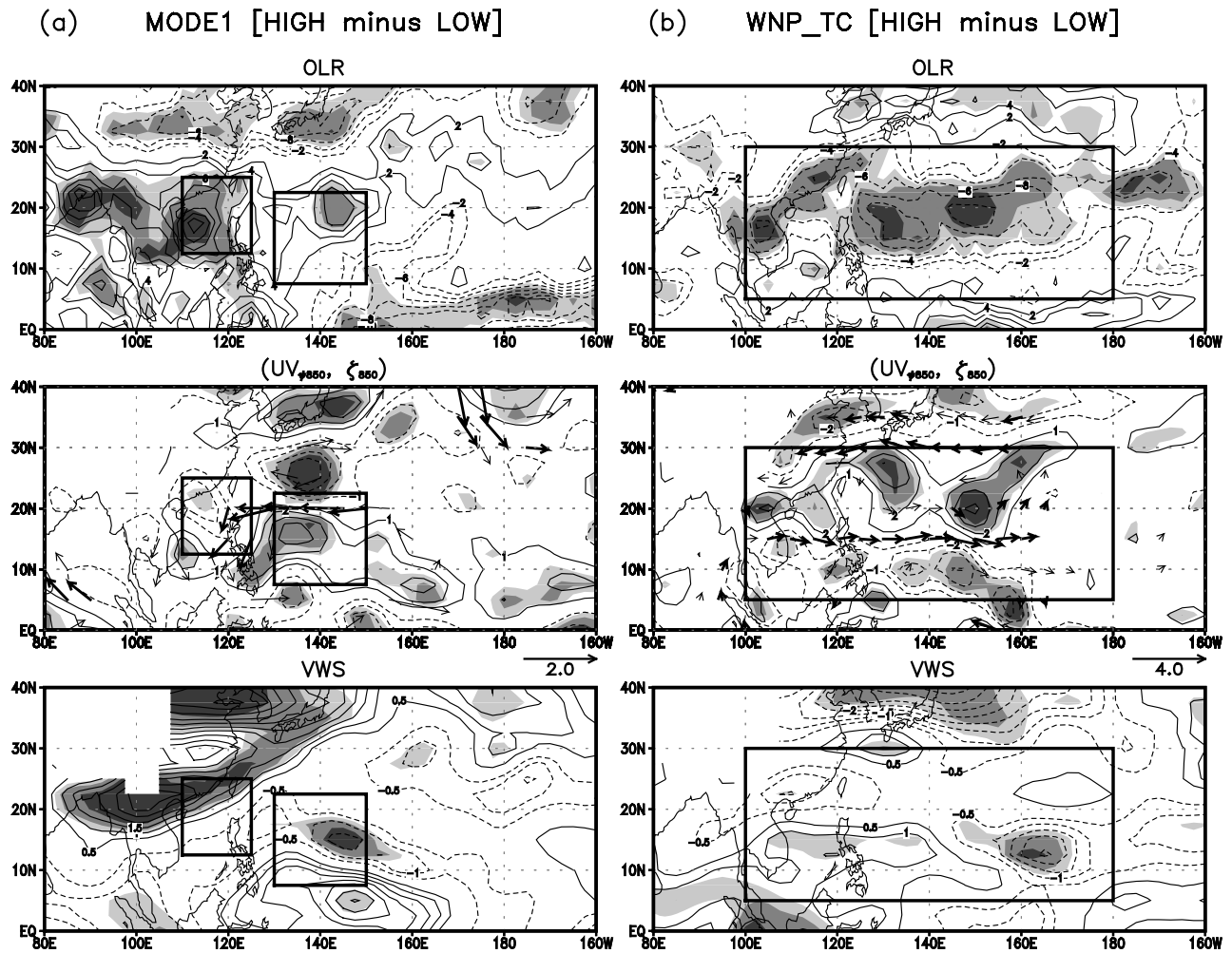


**Figure 15.** Same as Figure 14 except for (a) the PS-nSCS oscillation and (b) the basin-wide summertime WNP TC genesis.

corresponding organized anomalies in the center of boxed region. Accordingly, we conclude that the patterns of the SSTA associated with the decadal PS-nSCS oscillation (Figure 11a), as well as the decadal basin-wide TC genesis (Figure 11b) exert a stronger anomalous forcing to the tropical WNP. Additionally, the composite differences with respect to the raw time series are shown in Figure 15. With regard to the PS-nSCS oscillation, all the anomalous patterns clearly demonstrate combinations of the interannual and decadal time scales (Figure 15a). On the other hand, the anomalies consistent with the variability of TC genesis are well organized along the latitudinal belt between  $10^{\circ}$ – $30^{\circ}$ N in the composite differences between high and low years of the basin-wide summertime TC genesis (Figure 15b). These anomalies in large-scale environments are arisen from the anomalous zonal SST gradient in the subtropics along the latitudinal belt of  $10^{\circ}$ – $30^{\circ}$ N (figure not shown).

[31] The composite maps of total fields of the low-tropospheric circulation and the locations of TC genesis are also plotted with respect to the decadal PS-nSCS oscillation to confirm the dipolar redistribution of TC genesis on the decadal time scale between the two regions (Figure 16). The

overall results are analogous to those shown in Figure 10 in terms of the interannual variability. The monsoon trough is more (less) cyclonic in the PS and the subtropical ridge is more (less) anticyclonic along the  $30^{\circ}$ N during the high (low) years, but there is not clear difference in the nSCS, which was already expected from the vorticity anomalies in Figure 14a. Corresponding to the circulation pattern, the TC genesis frequency shows dipolar redistribution as well: 88 per 15 year (46 per 7 year) in the PS versus 33 per 15 year (16 per 7 year) in the nSCS for the thresholds of  $\pm 0.5\sigma$  ( $\pm 1.0\sigma$ ) during the high years, and 46 per 13 year (18 per 6 year) in the PS versus 54 per 13 year (28 per 6 year) in the nSCS during the low years. Note that the redistribution is less clear during the low years due to the number of geneses in the nSCS does not increase dramatically.

## 5. Summary and Concluding Remarks

[32] To address the three questions posed at the beginning of this paper, we obtained results that can be summarized as follows. In an attempt to understand the sub-basin-scale

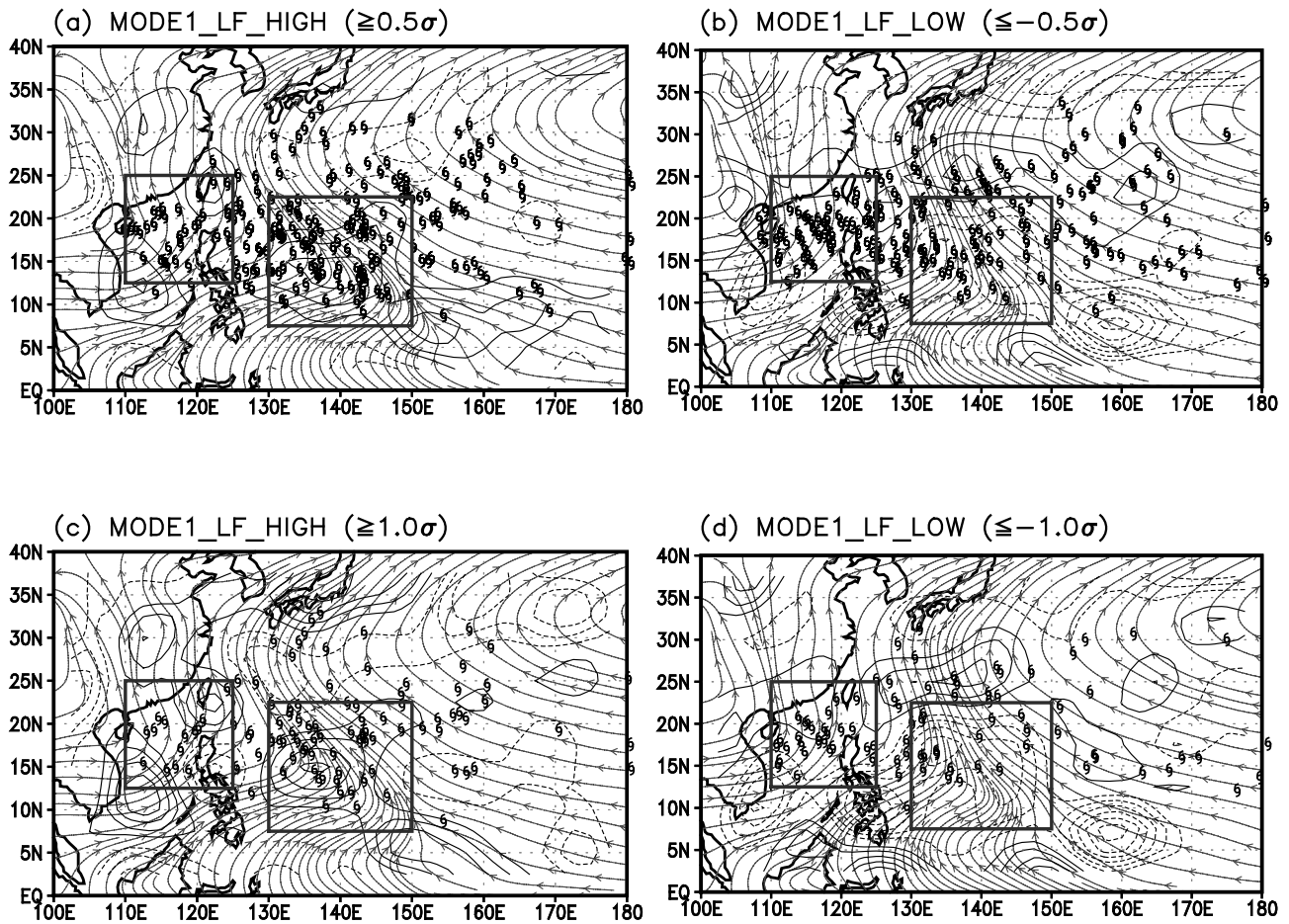


**Figure 16.** Same as Figure 10 except for the low-pass-filtered PS-nSCS oscillation.

decadal redistribution of WNP TC genesis, we found that the dipole oscillation between the PS (R1) and the nSCS (R2) is representative of such variability (Figure 3a).

[33] Even though the questions were given only for the decadal time scale, the interannual variability of the PS-nSCS dipole oscillation was also intriguing, and thus addressed in detail. We found that the interannual variability of the PS-nSCS oscillation is partly associated with the ENSO decaying periods, i.e., about half of the total events (i.e., 11/23) occurred after the wintertime ENSO event (Figure 8). Interestingly, this percentage is only slightly less than that related to the typical ENSO-related oscillation (Figure 3b, i.e., 12/21), even though the large-scale environmental patterns associate with the typical ENSO-related oscillation are much stronger (Figure 9). The asymmetry between El Niño and La Niña could explain this result; there were more events corresponding to the typical ENSO-related oscillation during the El Niño developing years (i.e., 6/8) than during the La Niña developing years (i.e., 6/13); that is, less coherency during the La Niña developing years decreased the percentage of the connection of this oscillation with the ENSO event. More robust relation with the El Niño episode resulted in the robust successive temporal relation (i.e., the high phase of the typical ENSO-related oscillation in the previous year leads to the low phase of the PS-nSCS oscillation in the following year) before and after the four conventional El Niño episodes (i.e., 1972–1973,

1982–1983, 1987–1988, and 1997–1998). This, in turn, suggests if there should be a strong El Niño episode, the low phase of the PS-nSCS oscillation; that is, more geneses in the nSCS than in the PS would be very likely to occur in the following summer TC season.

[34] On the decadal time scale, we found that the decadal CP SST warming, with its equatorial center of variability near the Niño-4 region, occurs when TC genesis was decadal enhanced in the PS and simultaneously suppressed in the nSCS (Figure 11a). Its time series was tolerably congruent with the decadal component of EMI, negative TNI and ZGSST index (Figure 13 and Table 1), indicating a possible role of decadal variation in the ENSO transition or recently emerged ENSO Modoki on modulating the decadal PS-nSCS redistribution of seasonal TC genesis. The actual forcing exerted to the WNP region to modulate the decadal PS-nSCS oscillation was interpreted mainly through the ZGSST between the equatorial WP and CP regions because this index showed the highest explained variance with the decadal PS-nSCS oscillation as well as with the decadal EMI (Table 1). The weaker equatorial ZGSST, which stands for the equatorial CP warming and WP cooling, has a positive effect on the weaker trade wind in the WNP. As a result, a low-tropospheric cyclonic vorticity and a weaker vertical wind shear form in R1, and simultaneously the strong positive OLR anomalies form in R2 (Figure 14a). These large-scale responses resulted

in the positive phase of the decadal PS-nSCS oscillation. Interestingly, these descriptions were very similar to those explaining the decadal variation in basin-wide WNP TC genesis. The different responses in the spatial variation of TC genesis certainly originated from the different patterns of the tropical Pacific SSTA; the decadal PS-nSCS oscillation resulted from the near equatorial SSTA, whereas the decadal variation in basin-wide TC genesis from the off-equatorial SSTA. However, the reason why the off-equatorial SSTA in the WP and CP regions exerted a forcing to the WNP with such a wider extent that was enough to modulate basin-wide TC genesis needs to be explored in a further study.

[35] Because observations have been limited to date, it is not entirely confident to say that the discovered relationship between the decadal PS-nSCS oscillation and the decadal ENSO Modoki or the transitional phase of ENSO will be robustly kept in the future as strong as in the analysis period. However, the change in the decadal ZGSST formed by the equatorial WP and CP SSTA can be interpreted as an actual forcing exerted to the WNP region that directly explains the decadal PS-nSCS oscillation. Thus, as long as the decadal ZGSST index shows higher in its relationship with the decadal EMI (or TNI) rather than with the decadal Niño-3 index (Table 1), the decadal PS-nSCS oscillation will have a largest variance congruent with the decadal EMI and TNI.

[36] **Acknowledgments.** This study was supported by CATER 2006-4204. We are grateful to three anonymous reviewers for their constructive suggestions and comments that led to improvement of this paper. J.H.K. thanks J. Heming for his helpful comments in the initial version. NCEP Reanalysis data, NOAA ERSST V2 data, and Interpolated OLR data provided by the NOAA/OAR/ESRL PSD, Boulder, Colorado, United States, from their Web site at <http://www.cdc.noaa.gov/>.

## References

- Ashok, K., S. K. Behera, S. A. Rao, H. Weng, and T. Yamagata (2007), El Niño Modoki and its possible teleconnection, *J. Geophys. Res.*, *112*, C11007, doi:10.1029/2006JC003798.
- Barlow, M., S. Nigam, and E. H. Berbery (2001), ENSO, Pacific decadal variability, and U.S. summertime precipitation, drought, and stream flow, *J. Clim.*, *14*, 2105–2128, doi:10.1175/1520-0442(2001)014<2105:EPDVAU>2.0.CO;2.
- Camargo, S. J., and A. H. Sobel (2005), Western North Pacific tropical cyclone intensity and ENSO, *J. Clim.*, *18*, 2996–3006, doi:10.1175/JCLI3457.1.
- Chan, J. C. L. (2006), Comments on “Changes in tropical cyclone number, duration, and intensity in a warming environment”, *Science*, *311*, 1713, doi:10.1126/science.1121522.
- Chan, J. C. L. (2008), Decadal variations of intense typhoon occurrence in the western North Pacific, *Proc. R. Soc. A*, *464*, 249–272, doi:10.1098/rspa.2007.0183.
- Chan, J. C. L., and K. S. Liu (2004), Global warming and western North Pacific typhoon activity from an observational perspective, *J. Clim.*, *17*, 4590–4602.
- Chang, C.-W., H.-H. Hsu, C.-R. Wu, and W.-J. Sheu (2008), Interannual mode of sea level in the South China Sea and the roles of El Niño and El Niño Modoki, *Geophys. Res. Lett.*, *35*, L03601, doi:10.1029/2007GL032562.
- Chu, P.-S. (2004), ENSO and tropical cyclone activity, in *Hurricanes and Typhoons: Past, Present, and Potential*, edited by R. J. Murnane and K. B. Liu, pp. 297–332, Columbia Univ. Press, New York.
- Di Lorenzo, E. et al. (2008), North Pacific Gyre Oscillation links ocean climate and ecosystem change, *Geophys. Res. Lett.*, *35*, L08607, doi:10.1029/2007GL032838.
- Duchon, C. E. (1979), Lanczos filtering in one and two dimensions, *J. Appl. Meteorol.*, *18*, 1016–1022, doi:10.1175/1520-0450(1979)018<1016:LFOAT>2.0.CO;2.
- Graham, N. E. (1994), Decadal-scale climate variability in the tropical and North Pacific during the 1970s and 1980s: Observations and model results, *Clim. Dyn.*, *10*, 135–162, doi:10.1007/BF00210626.
- Ho, C.-H., J.-J. Baik, J.-H. Kim, D.-Y. Gong, and C.-H. Sui (2004), Interdecadal changes in summertime typhoon tracks, *J. Clim.*, *17*, 1767–1776, doi:10.1175/1520-0442(2004)017<1767:ICISTT>2.0.CO;2.
- Kalnay, E., et al. (1996), The NCEP/NCAR 40-year reanalysis project, *Bull. Am. Meteorol. Soc.*, *77*, 437–471, doi:10.1175/1520-0477(1996)077<0437:TNYRP>2.0.CO;2.
- Kim, J.-H., C.-H. Ho, C.-H. Sui, and S. K. Park (2005), Dipole structure of interannual variations in summertime tropical cyclone activity over East Asia, *J. Clim.*, *18*, 5344–5356, doi:10.1175/JCLI3601.1.
- Klein, S. A., B. J. Soden, and N.-C. Lau (1999), Remote sea surface temperature variations during ENSO: Evidence for a tropical atmospheric bridge, *J. Clim.*, *12*, 917–932, doi:10.1175/1520-0442(1999)012<0917:RSSTVD>2.0.CO;2.
- Lander, M. A. (1994), An exploratory analysis of the relationship between tropical storm formation in the western North Pacific and ENSO, *Mon. Weather Rev.*, *122*, 636–651, doi:10.1175/1520-0493(1994)122<0636:AEAOTR>2.0.CO;2.
- Liebmann, B., and C. A. Smith (1996), Description of a complete (interpolated) outgoing longwave radiation dataset, *Bull. Am. Meteorol. Soc.*, *77*, 1275–1277.
- Liu, K. S., and J. C. L. Chan (2008), Interdecadal variability of western North Pacific tropical cyclone tracks, *J. Clim.*, *21*, 4464–4476, doi:10.1175/2008JCLI2207.1.
- Lohmann, K., and M. Latif (2005), Tropical Pacific decadal variability and the subtropical-tropical cells, *J. Clim.*, *18*, 5163–5178, doi:10.1175/JCLI3559.1.
- Mantua, N. J., S. R. Hare, Y. Zhang, J. M. Wallace, and R. C. Francis (1997), A Pacific interdecadal climate oscillation with impacts on salmon productions, *Bull. Am. Meteorol. Soc.*, *78*, 1069–1079, doi:10.1175/1520-0477(1997)078<1069:APICOW>2.0.CO;2.
- Matsuura, T., M. Yumoto, and S. Iizuka (2003), A mechanism of interdecadal variability of tropical cyclone activity over the western North Pacific, *Clim. Dyn.*, *21*, 105–117, doi:10.1007/s00382-003-0327-3.
- Nakamura, H., G. Lin, and T. Yamagata (1997), Decadal climate variability in the North Pacific during the recent decades, *Bull. Am. Meteorol. Soc.*, *78*, 2215–2225, doi:10.1175/1520-0477(1997)078<2215:DCVITN>2.0.CO;2.
- North, G. R., T. L. Bell, R. F. Cahalan, and F. J. Moeng (1982), Sampling errors in the estimation of empirical orthogonal functions, *Mon. Weather Rev.*, *110*, 699–706, doi:10.1175/1520-0493(1982)110<0699:SEITEO>2.0.CO;2.
- Smith, T. M., and R. W. Reynolds (2004), Improved extended reconstruction of SST (1854–1997), *J. Clim.*, *17*, 2466–2477, doi:10.1175/1520-0442(2004)017<2466:IEROS>2.0.CO;2.
- Trenberth, K. E., and J. W. Hurrell (1994), Decadal atmosphere-ocean variations in the Pacific, *Clim. Dyn.*, *9*, 303–319, doi:10.1007/BF00204745.
- Trenberth, K. E., and D. P. Stepaniak (2001), Indices of El Niño evolution, *J. Clim.*, *14*, 1697–1701, doi:10.1175/1520-0442(2001)014<1697:LIOENO>2.0.CO;2.
- Wang, B., and J. C. L. Chan (2002), How strong ENSO events affect tropical storm activity over the western North Pacific, *J. Clim.*, *15*, 1643–1658, doi:10.1175/1520-0442(2002)015<1643:HSEEA>2.0.CO;2.
- Weng, H., K. Ashok, S. K. Behera, S. A. Rao, and T. Yamagata (2007), Impacts of recent El Niño Modoki on dry/wet conditions in the Pacific rim during boreal summer, *Clim. Dyn.*, *29*, 113–129, doi:10.1007/s00382-007-0234-0.
- Wu, L., B. Wang, and S. Geng (2005), Growing typhoon influence on east Asia, *Geophys. Res. Lett.*, *32*, L18703, doi:10.1029/2005GL022937.
- Xie, S.-P., K. Hu, J. Hafner, H. Tokinaga, Y. Du, G. Huang, and T. Sampe (2009), Indian Ocean capacitor effect on Indo-western Pacific climate during the summer following El Niño, *J. Clim.*, *22*, 730–747, doi:10.1175/2008JCLI2544.1.
- Yumoto, M., and T. Matsuura (2001), Interdecadal variability of tropical cyclone activity in the western North Pacific, *J. Meteorol. Soc. Jpn.*, *79*, 23–35, doi:10.2151/jmsj.79.23.
- Zhang, C., and H. H. Hendon (1997), Propagating and standing components of the intraseasonal oscillation in tropical convection, *J. Atmos. Sci.*, *54*, 741–752, doi:10.1175/1520-0469(1997)054<0741:PASCOT>2.0.CO;2.

P.-S. Chu, Department of Meteorology, School of Ocean and Earth Science and Technology, University of Hawai‘i at Manoa, 2525 Correa Rd., HIG 350, Honolulu, HI 96822, USA.

C.-H. Ho, School of Earth and Environmental Sciences, College of Natural Sciences, Seoul National University, Seoul 151-747, South Korea.  
J.-H. Kim, Met Office Hadley Centre, FitzRoy Road, Exeter EX1 3PB, UK. (joo-hong.kim@metoffice.gov.uk)